STYRELSEN FÖR

VINTERSJÖFARTSFORSKNING

WINTER NAVIGATION RESEARCH BOARD

Research Report No 99

Mihkel Kõrgesaar and Pentti Kujala

VALIDATION OF THE PRELIMINARY ASSESMENT REGARDING THE OPERATIONAL RESTRICTIONS OF SHIPS ICE-STRENGHTENED IN ACCORDANCE WITH THE FINNISH-SWEDISH ICE CLASSES WHEN SAILING IN ICE CONDITIONS IN POLAR WATERS

Finnish Transport Safety Agency

Finnish Transport Agency

Finland

Swedish Maritime Administration

Swedish Transport Agency

Sweden

Talvimerenkulun tutkimusraportit — Winter Navigation Research Reports
ISSN 2342-4303
ISBN 978-952-311-224-7

FOREWORD

In this report no 99, the Winter Navigation Research Board presents the results of the research project IceSafety. The main objective of the project was to assess the validity of the preliminary operational restrictions according to the International Code for Ships Operating in Polar Waters (Polar Code) for ships ice-strengthened in accordance with the Finnish-Swedish Ice Class Rules (FSICR). Also, the accidental limit state of hull plating and frames according to FSICR was assessed and analysed. Full-scale measurement results were used in the assessment.

The Winter Navigation Research Board warmly thanks Mihkel Kõrgesaar and Pentti Kujala for this report.

Turku

October 2017

Jorma Kämäräinen

Finnish Transport Safety Agency

Tomas Årnell

Swedish Maritime Administration

Markus Karjalainen

Finnish Transport Agency

Stefan Eriksson

Swedish Transport Agency

Acknowledgements

The authors would like to gratefully acknowledge the funding support from Finnish Transport Safety Agency (TRAFI). We would like to thank Prof. Jani Romanoff for many valuble comments and suggestions made during the course of this work. We would also like to thank CSC – IT Centre for Science Ltd. for providing Abaqus package license and Reijo Lindgren from SIMULIA Finland for many valuable discussions regarding modelling issues.

Espoo, 31 January 2017
Mihkel Kõrgesaar & Pentti Kujala

Contents

1. Objectives

IMO has adopted the International Code for Ships Operating in Polar Waters (Polar Code) and related amendments to make it mandatory under both the International Convention for the Safety of Life at Sea (SOLAS) and the International Convention for the Prevention of Pollution from Ships (MARPOL). The Polar Code entered into force on 1 January 2017. To analyse the application of the Polar Code for the Finnish-Swedish Ice Classes, the following work was done by Aalto University:

- The main objective of the study is to assess the validity of the preliminary assessment of the operational restrictions for ships ice-strengthened in accordance with different Finnish-Swedish Ice Classes. The assessment shall be done separately for independent operation in ice and operation with icebreaker assistance. A preliminary assessment can be found in section 8, 'Safe operational ice conditions for ships ice-strengthened in accordance with FSICR', of Appendix 3 of the document MSC 94/INF.13 (2014) 'Description of the Finnish-Swedish Ice Class Rules and their operational limitations'. This section is given also in Appendix A.
- The other objective is to assess and analyse the accidental limit state of ship hull structures designed in accordance with the Finnish-Swedish Ice Class Rules (2010), particularly of that of frames and plating. The aim is to determine the strength levels of ice-strengthened framing and plating, which are subject to local loads imposed by ice. In addition to simplified analytical equations used in class rules, state of the art design tools, such as finite element method, would be used to assess the accidental limit state. The investigation will show the safety margin with respect to accidental limit state as defined in the present rules.
- The assessment will be based on relevant full scale ice load measurements (such as MT Uikku data form the Kara Sea during April 1998 with navigation behind an icebreaker and SA Agulhas II data from the Antarctica 2013-2016 representing a ship with independent navigation) and available damage data of ships which have sailed in ice conditions in Polar areas and other ice-covered sea areas.
- Comparison of the results of strength analyses with the POLARIS system (Methodogy for assessing operational capabilities and limitations in ice: Polar Operational Limit Assessment Risk Indexing System (POLARIS)).

2. Introduction

Knowledge about the structural response under the expected loading – local ice loads from first year ice in this case – is required for the evaluation of the design point. The knowledge of the loading includes quantities describing the load (pressure and the load patch dimensions) as well as the statistics of the loading.

The structural response investigated here includes only the response of the local structures, i.e. the structural members of the shell of the ship hull. Thus, the investigation is restricted to plating and frames. A further restriction is to investigate only transversely framed structures as knowledge about ice loading statistics for longitudinally framed structures is limited. The structural response formulations used in the analysis are obtained from literature for both the elastic response and the plastic response.

Current design methods of ships entering ice-covered waters are based on experience and ice load measurements from small ships (ISSC, 2015). Therefore, design practice for the design and analysis of ice-classed ship structures is to assume a stationary, uniform pressure loads (FSICR, 2010), or loads resulting from a glancing impact with an ice edge (IACS, 2011). The credibility of this practice has been under examination lately in several studies indicating that uniform and/or stationary loads might yield conservative results compared with actual measured field data (Quinton et al. 2010; 2012, Erceg et al. 2014, Kõrgesaar and Kujala 2016). Their findings suggest that high degree of spatial and temporal variations observed in ice load measurements, the so-called *high pressure zones*, can more easily lead to permanent deformations in ship structures.

This is important considering that FSICR are the most commonly applied design standards for ice-strengthened ships in the Baltic waters, although most of the assumptions made in the rules are based on empirical experience. FSICR does not explicitly specify acceptable permanent deformation and safety margin of shell plating and framing. In addition, there are high level of uncertainties associated with design ice loads in FSICR. The ice loads defined in direct calculation guidelines using FSICR are not extreme ice loads as the design philosophy of the FSIRC rules is to use annual maximum ice loads and determine the scantlings using first yield as a limit state (Riska and Kämäräinen 2011). Consequently, measured maximum ice loads are about 3 times larger than the design ice loads defined in the ice class rules. Furthermore, finite element analyses by Lyngra (2014) showed that the rules also exhibit conservative design margin with a substantial load carrying capacity beyond the design load level. Hence, these rules were deemed unsuitable for calculation of load carrying capacity of a structure (Lyngra, 2014), which is understandable as the first yield is the limit state in the current FSIRC approach.

To address these gaps in the rules, a more realistic evaluation of structural performance using non-linear finite element analyses is performed.

3. Loading

To explore the capacity of the ice strengthened frames and structures, which behavior at larger load levels might be significantly influenced by the load distribution, it is important to characterize the load properly. Therefore, the objective of this chapter is to review the design load compliant with FSICR and point out some of the possible weaknesses of that approach. To bypass those weaknesses, we propose an alternative loading scenario. Comparison of different loading scenarios is made in the following sections.

3.1 Design load according to FSICR

As the ice load is a statistical quantity, the design load needs to be determined by an assumption of probability level or return period of the load (Riska, 2014). The load level defined in the present FSICR is determined based also on the experience of ice-induced hull damage. Therefore, the loading should be viewed together with the allowed response (yield point or plastic deformation). This enables the loading probability and the expected response to be in balance.

Ice load definition is a significant part of the hull rules. For the purpose of structural design, the standard procedure is an assumption that ice load can be described by uniform ice pressure, termed p_{av}, on a rectangular load patch of height h and length l (Riska, 2014). This approach of constant pressure is taken as the extreme material properties of the Baltic ice do not change much through the winter in different Baltic Sea areas. Therefore, the total force is $F = p_{av} \cdot h \cdot l$. The ice load definition in the FSICR is such that ice pressure is constant for all classes (nominal ice pressure p_0) and load height h is the class factor (ranging from 0.35 m for IA Super to 0.22 m for 1C).

The total ice load for each structural member is taken as the line load q times the load length l_a that depends on the distance between respective structural members (horizontal span or spacing). For transverse frames the load is, for example, $F = q \cdot s$, where s is the frame spacing.

The direct analysis of a large grillage structures is carried out using a load patch with p, h and patch length of webframe spacing. The load patch is to be applied at locations where the capacity of the structure under the combined effects of bending and shear are minimized. The analysis of results of SAFEICE project highlighted the fact that the design loads in the FSICR are relatively low – but in balance with the design point which is first yield.

3.1.1 Height of the ice load area

Another assumption is that the ice-strengthened ship operation is limited to open sea conditions corresponding to a level ice thickness h_o, see Table 1. The corresponding design ice load height h of the area subjected to ice pressure is assumed to be only a segment of the ice thickness.

Table 1. Load height for each ice class

Ice Class	h_o [m]	h [m]
IA Super	1.0	0.35
IA	0.8	0.30
IB	0.6	0.25
IC	0.4	0.22

3.1.2 Ice loading on different hull areas

In all ice class rules, the hull loading depends on the location of the hull where the loading is defined. The bow, mid body and stern encounter different loads. As the loads on different areas are of different origin, it is also evident that the loading magnitude is different. This is taken into account in the most ice rules by dividing the ship hull into areas and defining hull factors for each area. These hull area factors are related the loading of that particular area to that of the bow.

In the FSICR three hull areas are used: bow, mid body and stern. The loading is also assumed to be acting on narrow area in vertical direction. The strengthened area is called the ice belt. Each of the three hull regions has a design ice pressure defined by a hull region factor c_p. This factor is for the bow region and is scaled according to the ice class for other regions so that the stern region has the lowest design ice pressure. For ice class IC, the stern hull region coefficient is 0.25.

3.1.3 Influence of load length according to measurements

Another factor used to define the ice pressure is a coefficient dependent on the load length, c_a. Each structural member has an associated load length l_a – this is the length of the load that influences the response in the hull area.

The function relating measured maximum line load with loading length has been researched on e.g. by Suominen and Kujala (2015). The function, defined in eq. (1), is fitted to multiple ship measurement data to render curves denoting the magnitude of line load q as a function of load length.

$$q = C \left(\frac{l_c}{s}\right)^{-a} \text{[kN/m]} \quad (1)$$

where s is the frame spacing, l_c is the load length, C and a are unknown parameters specific to each ship.

The study included two data sets (Arctic and Antarctic) divided into one and twelve-hour time periods. The line load maxima were calculated for each time-period for the bow and stern. In each location of the ship hull, multiple load lengths were considered for these calculations which corresponded to the number of frame spacing. Results of this research demonstrate that Gumbel I asymptotic distribution gives a suitable representation of the measured maxima.

C and a are determined with non-linear least square method by curve-fitting with each ship's measurement data (Figure 1a). For the case of ship S.A. Agulhas II, s is 0.4m, the C is obtained as 1989 kN/m and a is 0.733 for the stern and 3150 kN/m and 0.538 for the bow. It has to be noted that the results naturally differ whether 1 or 12 hour maxima is employed when the return period of time is determined.

3.2 Alternative loading scenarios

The weak point of FSICR design pressure patch approach is that it excludes the combined effect of localized ice loading and load distribution over the longer horizontal area. Furthermore, as implied by the depiction in Figure 1 (b) the load length can considerably vary in practice, which should be considered by the rules. Moreover, the load along horizontal direction can vary with one frame carrying the highest load, while the load decreases with increasing distance from this

frame. The latter notion is supported also by measurements conducted on icebreaker Sisu (Kujala and Vuorio, 1986).

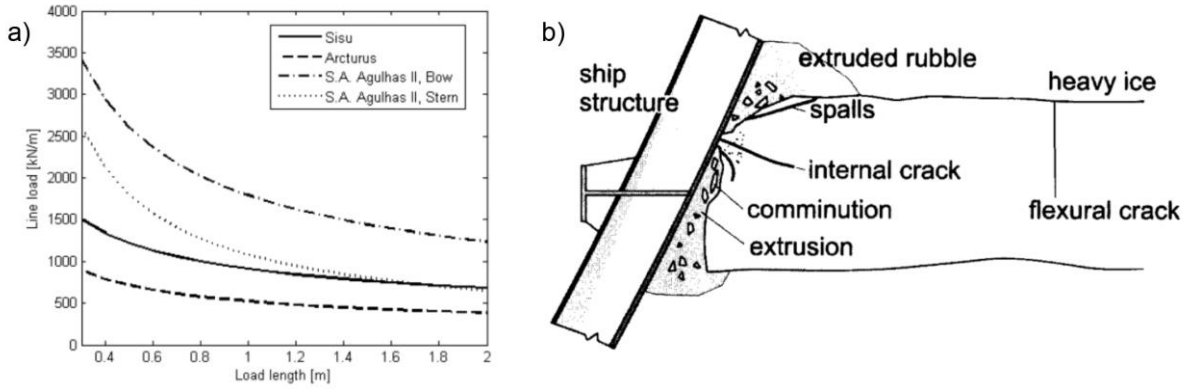

Figure 1. a) Maximum line loads determined from full-scale ship measurements (three ships) as a function of load length (Suominen and Kujala, 2015) – Return period taken is 10 days. b) Sketch of ice contact with ship structure – may describe an event that is only centimeters across, or it may be meters across, Daley (2007).

3.2.1 Load length effect

The present FSICR approach assumes that load is equally distributed between framing members and in direct analysis with FEM, pressure patch length equals the webframe spacing; e.g., see Figure 2, case 8s. To determine the effect of patch length on capacity of the frames four different loading scenarios are considered besides the uniform pressure patch of FSICR as shown in Figure 2. The length of the patch is decreased from webframe spacing (FSICR, denoted as 8s) to one frame spacing (1s). Furthermore, in the last case study a scenario is proposed where pressure is uniform over a frame spacing, but decreases exponentially outside this area as defined with eq. (1). This case is denoted as non-uniform pressure patch – NUPP.

$$p = \begin{cases} 8.7(7.175 - x)^{-0.733} \; if \; x < 6.285 \\ 18.8 \qquad\qquad if \; 6.825 \leq x \leq 7.175 \\ 8.7(x - 6.825)^{-0.733} \; if \; x > 7.715 \end{cases} \tag{2}$$

In contrast to FSICR, NUPP considers the fact that that ice load will have some local character in the middle, but also accounts the decreasing load character that is consistent with measurements shown in Figure 1 (a). This local charater is especially important when considering overload situations to which we focus in this report.

The pressure values shown in Figure 2 were chosen based on preliminary simulations so that plastic deformations would take place in the structure. Since in the simulations pressure is ramped up from zero to maximum the presented values are the maximum attained. The advantage of ramping procedure is that pressure can be treated as a variable when results are analyzed. Details of pressure application are presented in the next section.

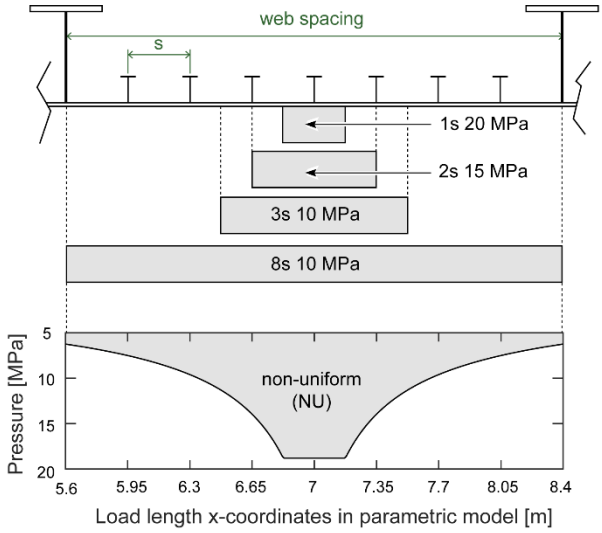

Figure 2. Pressure patches used in the investigation

3.2.2 Effect of load height

As the ship penetrates into an ice sheet, the ice edge is crushing and a nominal contact area is increasing – the process is depicted in Figure 3 (b) and its adoption is also basis for current design pressure patch height. The crushing of ice continues until the bending failure of the ice sheet. However, there is an aboundance of evidence that crushing phase contains an intermediate phenomenon whereby a "line-like" contact developes from adjacent of high pressure zones distributed over the contact region. The resulting scenario is also proposed as a possible future design scenario, see Figure 3 (c).

The pressure values measured in those localized zones can be as high as ~50 MPa, as opposed, ice pressure in FSICR is never higher than 5.6 MPa. This striking difference represents a significant gap in the knowledge and thus, also in the rules, which can only be addressed by seamless intertwining of experimental testing and numerical simulations. Current study focuses on the latter as simulations allow us to separate the individual and interactive effects of factors that have most deteriorating effect on the structural behaviour. Therfore, one of those individual effects we focus is load height, besides the load length.

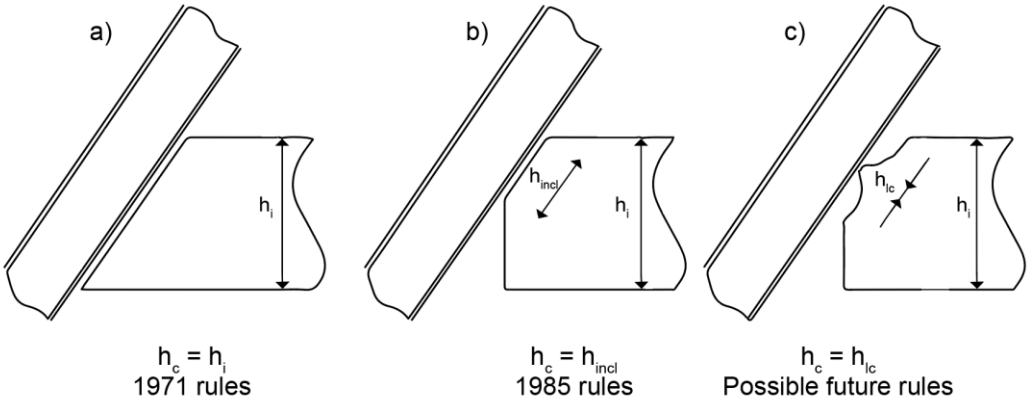

Figure 3. Load height development in FSICR (Riska and Kämäräinen, 2012).

4. FE analyses

4.1 Case study structure

As a case study structure, we selected M/T Uikku ship bow region. Ship is classified according to FSICR as ice class IA Super. Ship was built 1976 in Werft Nobiskrug Gmbh. Ship has a diesel electric propulsion system with four diesel generators. Details of the design are shown in Table 3.

4.2 FE modelling

Analyses are performed with a large 5-bay grillage structure shown in Figure 4. The reasoning behind the large model size was to reduce the effect of boundary conditions on the response. The boundary conditions on the model edge are defined so that all translations are fixed. We believe that this is more conservative than fixing all degrees of freedom as stiffness is reduced. Moreover, the uncertainty related with boundary conditions is somewhat relieved by the large chosen model size.

The pressure patches shown in Figure 2 are defined on the region with refined mesh of 50 mm between two webframes; rest of the model has the mesh size of 150 mm. In simulations one loading-unloading cycle took place. Pressure in the simulations was ramped up from zero to maximum value specified in Figure 2. The maximum pressure was reached at the half-point of the simulation, after which it linearly decreased back to zero. Because of unloading, we could determine the permanent plastic deformation in the structure. Similar procedure is advocated by the ABS (2014) guidance notes on ice class.

All FE simulations are performed with FE software ABAQUS 6.13-3. Modelled structures are discretized with reduced integration shell (S4R) elements with 5 integration points through thickness and stiffness based hourglass control. They possess six degrees of freedom on each node. Initially all simulations were set-up using implicit analysis procedure (ABAQUS/Standard) using Static step. However, some of the analysis stopped prematurely because convergence was not reached during the specified number of increments of 500 and minimum time increment of 1e-12; simulation time was 2 seconds. To overcome the increasing number of non-linearities in those cases, simulations were run using explicit analysis procedure (ABAQUS/Explicit) instead.

In explicit simulations, the analysis time was set to 5 seconds, which included both the loading and unloading cycle. The computational time was reduced by mass-scaling the entire model in the beginning of the analysis by a factor of 14. Despite this large factor, comparison with implicit non-mass scaled solution indicates that changes in the mass and consequent increases in the inertial forces do not alter the solution accuracy compared with implicit solution (Figure 4), nor does it increase the kinetic energy over the suggested limit value of 5% of total internal energy. Furthermore, numerical noise associated with dynamic effects was damped out using viscous pressure (2% of ρc_d, where c_d is the dilatational wave speed of the material) applied on the fine mesh region of the outer shell shown in Figure 4.

Two different true stress - plastic strain curves were used in the simulation to determine the effect of material non-linearity on the analysis results. The true stress-strain curve is highly non-linear in the plastic region, but can be approximated as linear in the practical ranges of structural deformation of interest here. Commonly the curve is approximated as a bi-linear curve with linear hardening with post yield modulus ranging from 0 to 2000 MPa (Abraham, 2008).

First, a non-linear material relation was employed determined with 3 mm thick tensile (dog-bone) specimens, see Figure 5. The material is a standard structural steel S235JR with following minimum values for mechanical properties defined in standard EN 10025-2: ReH = 235MPa, Rm = 360…510MPa and elongation after fracture of 26%. Second, a bi-linear elastic perfectly plastic material was defined with the same yield stress as non-linear material, 285 MPa.

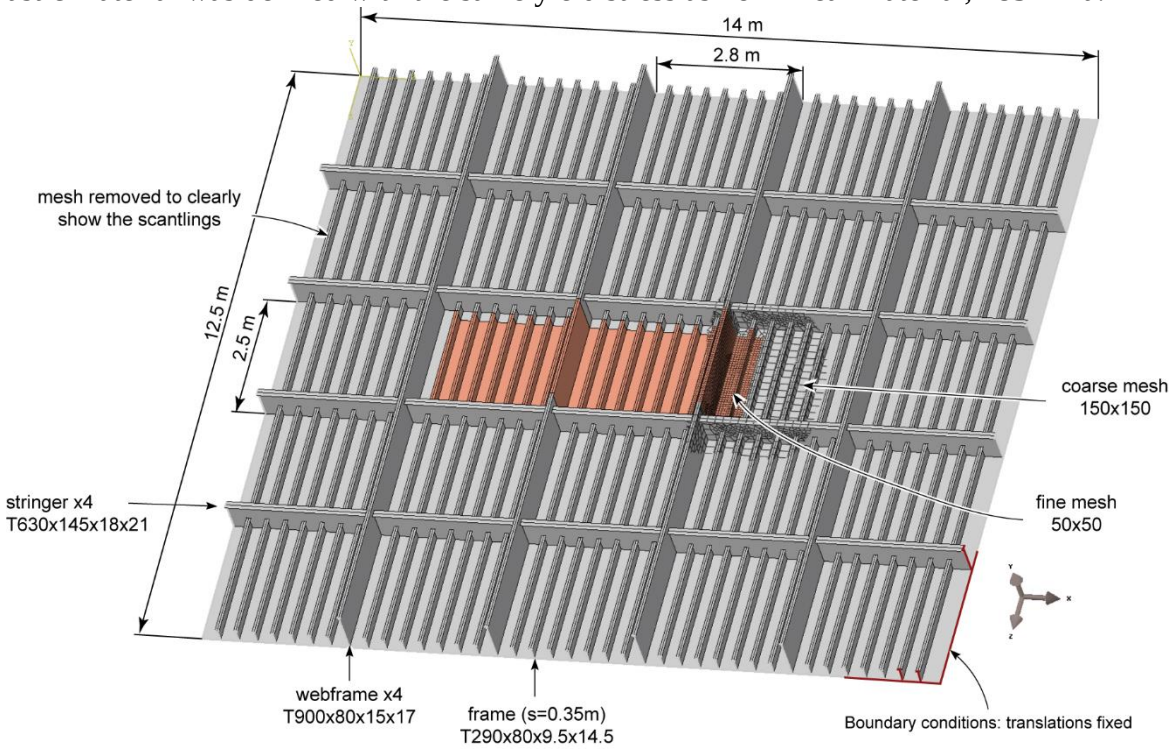

Figure 4. Five bay grillage FE model used in the analyses. Design scantlings correspond to Uikku bow designed according to FSICR IA Super. Plate thickness is 21.5 mm.

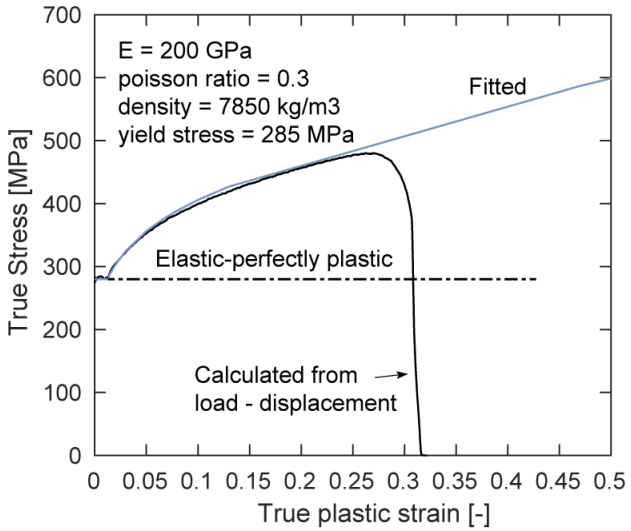

Figure 5. Material relations used in the simulation. Non-linear true stress-plastic strain curve determined with tensile tests and bi-linear elastic perfectly plastic approximation.

4.2.1 Load corresponding to displacement

In the analysis, the objective is to compare the capacity of the frames with respect to load that is necessary to reach permanent displacement equal to 1/12 of the frame spacing, i.e. serviceability limit state stipulated by DNV, Lepik *et al*. (2010). Naturally the load could not be defined

a priori so that after unloading permanent set is exactly equal to the reference limit state. That is why the pressure defined in Figure 2 is relatively large.

To determine the load corresponding to certain displacement we shifted the unloading portion of the curve so that the permanent set would be exactly equal to the reference permanent displacement as shown in Figure 60. The underlying assumption is that slope of the unloading portion of the curve remains the same due to the permanent nature of plastic strains. This assumption of similarity in unloading slope is verified with simulation where maximum pressure was decreased (case 3s, new max. pressure 5 MPa) in Figure 6 – the two slopes, calculated and shifted, overlap.

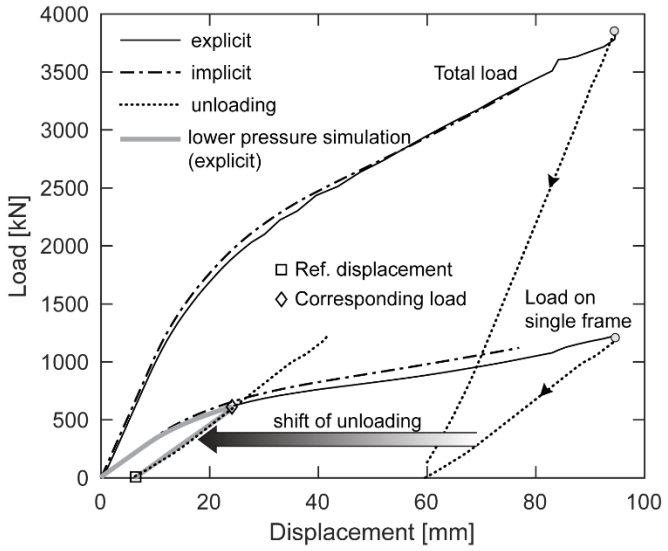

Figure 6. Comparison of implicit and explicit solution together with curve shifting verification. Results correspond to loading case 3s performed with non-linear material. Implicit simulation stopped before unloading stage started. Total load corresponds to resultant force in the boundaries. Load on frame is obtained by integrating the pressure over the single frame spacing.

4.3 Load length effect on response

Analyses results are shown in Figure 7 where load on a single frame is plotted as a function of displacement. Load on a single frame, that is for the one frame spacing, was found by integrating the applied pressure over the corresponding area. Displacements were measured at the two locations: 1) where it was highest in the plate field (Figure 7 a), and 2) in the plate field at the frame location (Figure 7 b). The capacity of the frames is compared with respect to load that is necessary to reach permanent displacement equal to 1/12 of the frame spacing, i.e. serviceability limit state stipulated by DNV. The procedure is described in previous section.

The results in Figure 70 (a) demonstrate that material non-linearity has negligible influence on the response in the range of structural deformations considered. The reason is that plastic strains remain small in the range below 5% at the permanent displacement limit used here, for example, see Figure 8. Using bi-linear material reduces the analysis set-up time, but the range of deformations where this simplification remains valid should be determined.

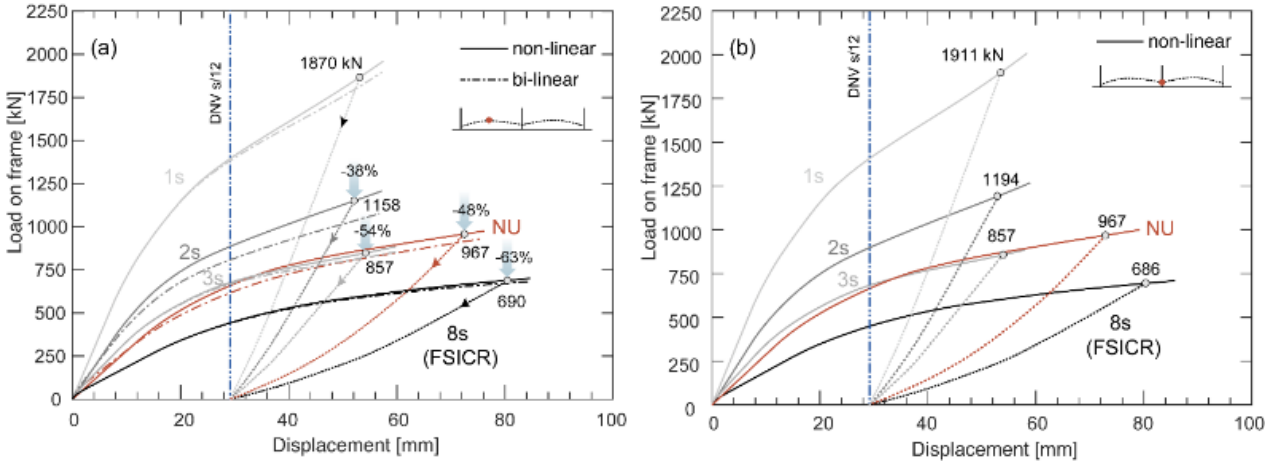

Figure 7. Load on single frame as a function of displacement. Displacement at (a) middle of the plate field and (b) on the plate field at the frame location. For each case load causing the permanent deformation of s/12 is highlighted.

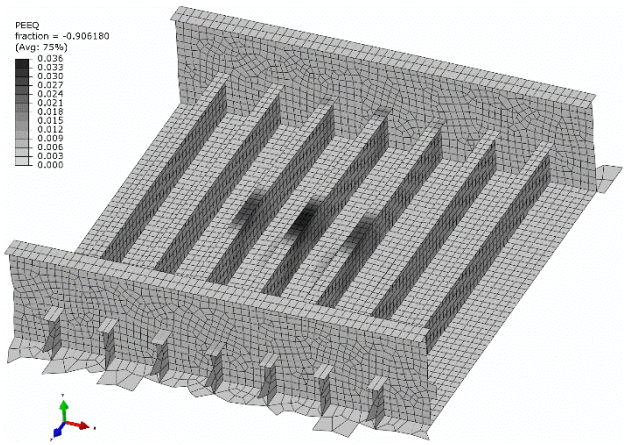

Figure 8. Excerpt of the structure under 3s patch at the instance when load on frame is 857 kN. Plastic strains remain under 4%.

Comparison of Figure 7 (a) and (b) shows that slightly stiffer response is obtained when deformations are measured at the frame location. But as the effect is negligible we focus on results presented in Figure 7 (a).

Results in Figure 7 (a) imply that capacity considerably reduces with increasing load length, rendering the current design approach the most critical (8s). But the impression is deceiving as the external loading acting outside the single frame spacing clearly reduces the structural stiffness of individual frames.

Therefore, to account for this effect we convert the determined load, F_{frame}, into format of line load and present it as a function of load length. For uniform load the calculated line load is

$$q_{un} = F_{frame}/s \tag{3}$$

where s is the frame spacing. For non-uniform load, the line load is found by integrating the pressure function given by eq. (1) and by normalizing it to account for the fact that F_{frame} was reached before maximum applied load was reached in the simulation

$$q_{nu} = \frac{h}{L}\int_{5.6}^{8.4} p(x)dx \cdot \frac{F_{frame}}{h\int_{6.825}^{7.175} p(x)dx} \tag{4}$$

$$= \frac{h}{L}\int_{5.6}^{8.4} p(x)dx \cdot \frac{F_{frame}}{18.8 \cdot h \cdot s}$$

where h = 0.35 m is the height of the patch, and L = 2.8 m is the length of the patch. The results are presented in Table 2. The obtained line load is also plotted against full-scale ship measurement data in Figure 9 for two ships. Although the measurement data applies to different structures, the comparison shows that the trend of the obtained results is consistent with the measured values. Qualitatively, the most critical loading scenarios are the ones in which percentage difference with measurements is smallest – cases 2s and 3s; in this comparison, we selected Agulhas II ship whose measurements better correlate with the calculated values. This percentage is also given in Table 2.

These results show that both the length of the pressure patch and the non-uniformity of pressure play an important role in determining the plastic capacity of the frames and thus, also the whole structure. If the shift in rules is made towards allowance of plastic limit states future FSICR rules should aspire to the patch definition that yields the most conservative results – largest damage with the least applied load. Comparison of critical line load values with the measured values in Figure 9 indicates that the current FSICR design approach is not the most critical scenario. Narrower patches or non-uniform pressure distribution are qualitatively more critical. Important perspective considering that recent findings indicate that load has to be in the range of (1-4 frame spacings) in order for the maximum load on a frame to occur, Suominen et al. (2017).

Table 2. Load on single frame to reach the permanent displacement equal to 1/12 of the frame spacing.

Case	solver	Load length [m]	Load on frame [kN] (F_frame)	Line load q1 [kN/m]	q2 [kN/m] Agulhass bow	(q1-q2)/q2 [%]
1s	implicit	0.35	1870	5343	3385	58 %
2s	implicit	0.7	1158	3309	2331	42 %
3s	explicit	1.05	857	2449	1874	31 %
8s	explicit	2.8	690	1971	1106	78 %
NU	implicit	2.8	967	1623	1106	47 %

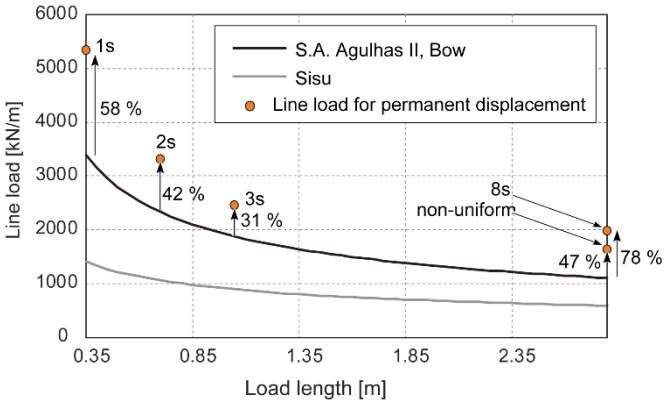

Figure 9. *Line load – load length* relationship determined from full-scale ship measurements (Suominen and Kujala, 2015). Return period taken is 10 days.

4.4 Effect of material hardening – large deformations

The effect of material hardening on the large deformation behaviour is further investigated, by using NUPP pressure patch on Uikku IA Super bow grillage.

The results of the analysis in Figure 10 (a) indicate that material hardening has negligible effect on the frame response, at least during majority of the response. This material insensitivity in large grillage is attributed to the structures ability to effectively distribute loads. Essentially there are two competing mechanisms taking place – material hardening and structural softening. Material hardening associated with localized plastic deformation remains so localized that it has negligible effect on the overall load-displacement response. To confirm this hypothesis analyses were performed also with an isolated frame, again using the same two material models. Figure 10 (b) reveals that in isolated frame the material has a stronger role on response.

Going back to large grillage, the closer inspection of deformed structures revealed an important disparity between two material modelling approaches at later stages of analysis, see Figure 11 where development of plastic strain is plotted in different stages of analysis. In simulations with non-linear material the hardening promotes distribution of stresses and plastic strains as opposed to local material deformation that requires more energy. In contrast, such mechanism is missing in simulations with bi-linear material. Plastic strains localize in frame flanges with very little spread that in turn leads to eventual neck development and failure. Furthermore, the inability to spread the stresses leads also to different structural behaviour with frames tripping and folding in simulations with non-linear material, but remaining straight in bi-linear material simulation.

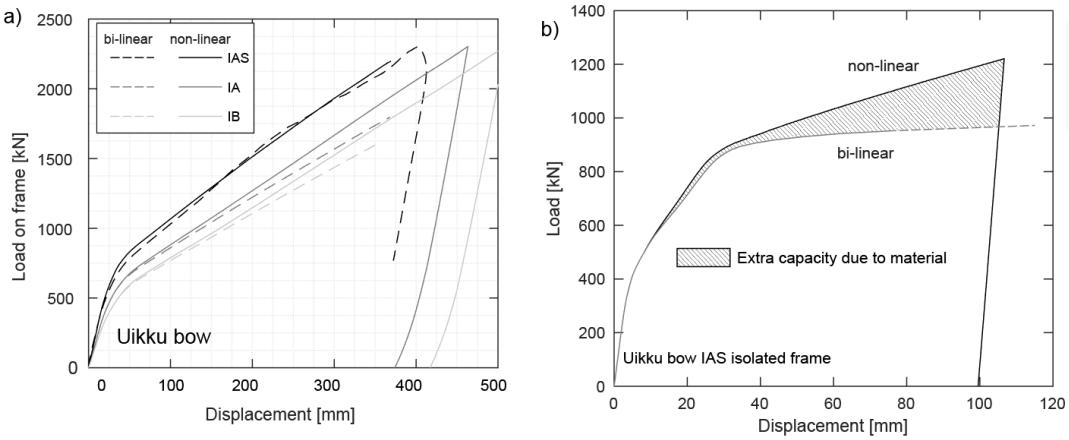

Figure 10. The effect of material non-linearity on Uikku bow frame response. a) Grillage and b) isolated frame.

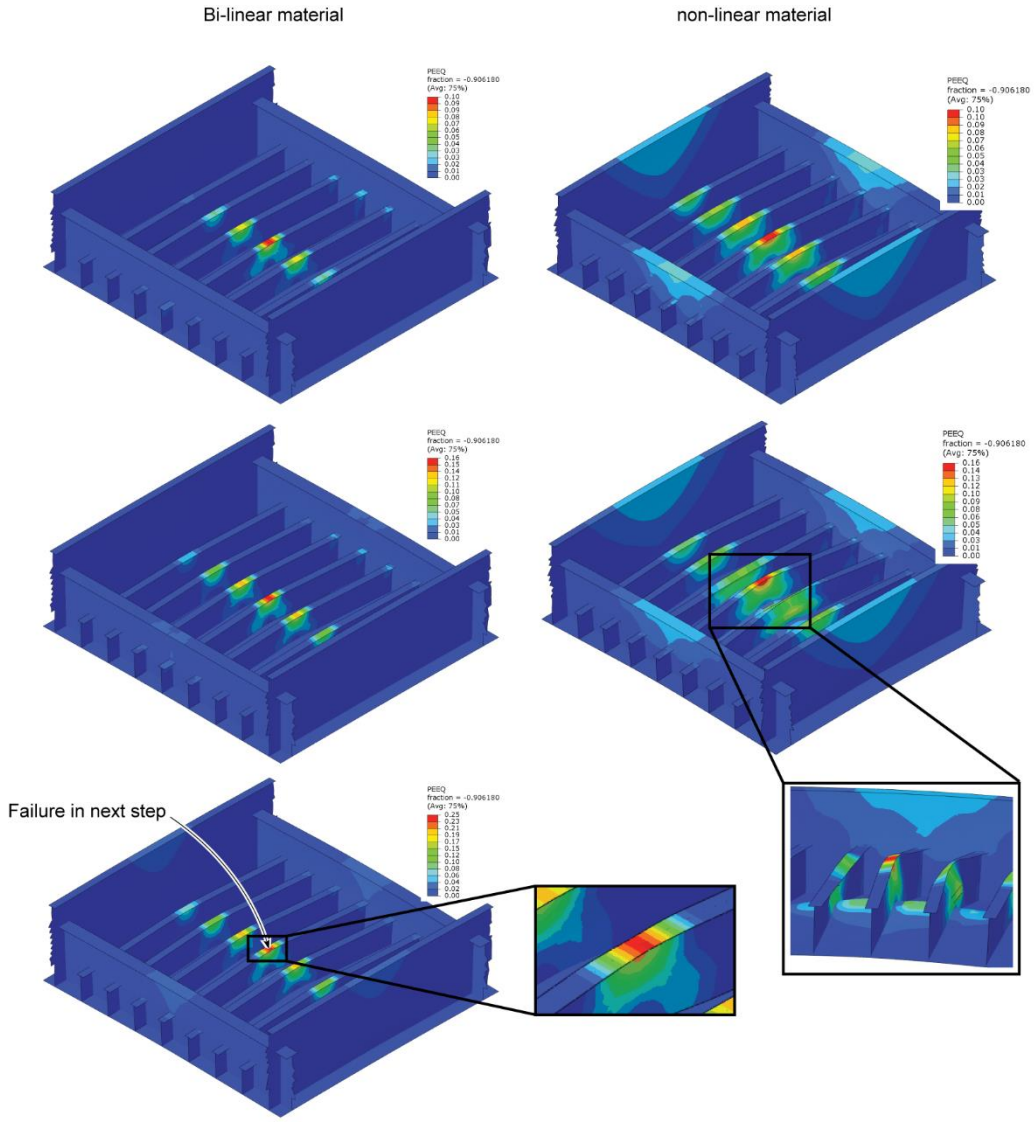

Figure 11. Effect of material non-linearity on plasticity spread in structures.

4.5 Effect of load height

To test the effect of load height on the analysis results two patch heights are considered: 35 cm consistent with IA Super current design patch and 10 cm height. Again, the structure of Uikku bow IA Super is employed for the analysis. The pressure distribution in the horizontal direction was non-uniform according to NUPP with the length of webframe distance defined in previous section.

Simulations were set-up so that the total load would be equal in both cases, which implies that the pressure applied through the narrower patch is about 3.5 times higher. In terms of the whole structure, this pressure difference has negligible effect on response as shown in Figure 12 (a). Much more revealing insight is obtained when inspecting the single frame response in Figure 12 (b). Under the same nominal load, the localization created by the “line-like” load significantly reduces the capacity of the frame. The load on frame causing permanent deformation of ~50 mm is about two times lower than manifested through patch with height of 35 cm.

As the effect of load height prominently reduces the capacity of the frames, more compelling, experimental insight is needed before enforcing load height change in rules. Therefore, the following analysis are performed with load height consistent with the current rules.

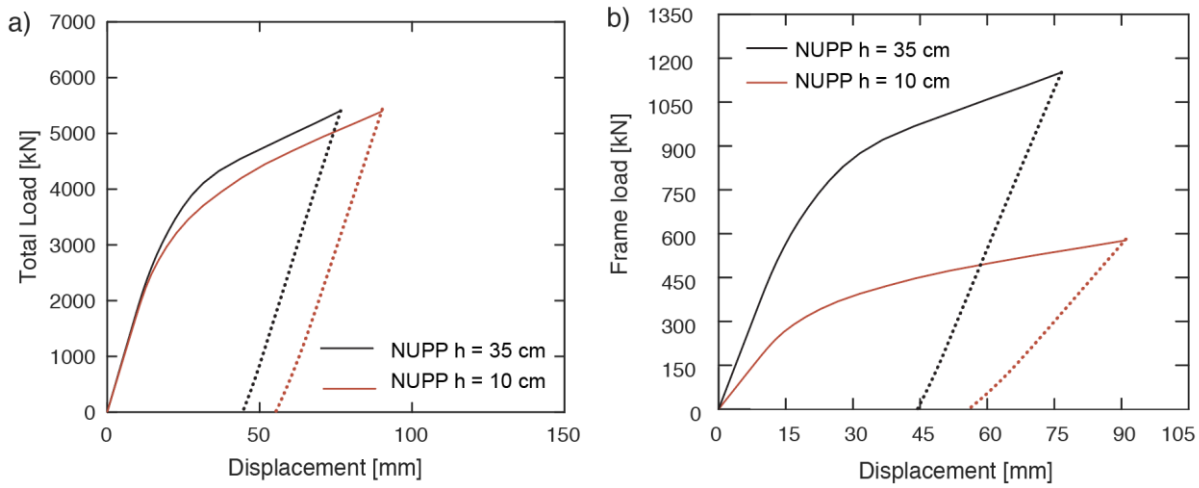

Figure 12. Effect of patch height on the response. a) Effect on structure and b) on single frame.

5. Fracture limit state

The objective of this section is to determine how and where fracture takes place in side structure under distributed pressure load. Although the load corresponding to the pressure patch area might be unrealistically high, the analyses are in agreement with the current best practice and are still believed to give important insight regarding fracture behaviour as well as structural behaviour prior to failure. Furthermore, of interest are the load values at which fracture takes place so these can be compred with values presented in Table 5.

5.1 FE simulations including fracture

Fracture in the material was modeled by deleting elements when fracture strain, independent of stress state, was reached. Although fracture strain in metals strongly depends on the stress state, this coarse assumption is justified by the fact that the objective here is to determine the structural component prone to fracture initiation under pressure loads in contrast to fracture propagation analysis. Fracture strain was scaled with element size. There are several equations developed for this purpose. Usually they are based on Barba's relation that is formulated as follows (Hogström 2009)

$$\varepsilon_f = \ln\left(e^{\varepsilon_n} + c\frac{\sqrt{Wt}}{L_{VE}}\right) \tag{5}$$

Here, ε_f is fracture strain, ε_n (0.2) equals to necking strain of the material estimated from engineering stress-strain curve, c (0.164, determined from fit on data) is the Barba parameter and W (15mm) and t (3mm) represent original width and thickness of flat tensile test specimen, respectively. L_{VE} is the length of the virtual extensometer (VE) over which fracture strain is measured in a tensile test. For 50 mm elements used in the present investigation, eq. (5) yields a fracture strain of 0.26.

Analyses were performed with Uikku mid-section model designed according to IAS and IB ice classes. The results are presented in Figure 13. In both cases fracture initates in the frame flange, whereas at the point of failure plastic strain in the outer shell is around 14%. The displacement to failure is ~0.5 m, which compared to the permanent deflection limit state used in

previous section (30 mm) is about 16 times higher. Load to fracture in case of IAS is ~2500 kN is about 5 times higher, again compared with permanent deflection LS.

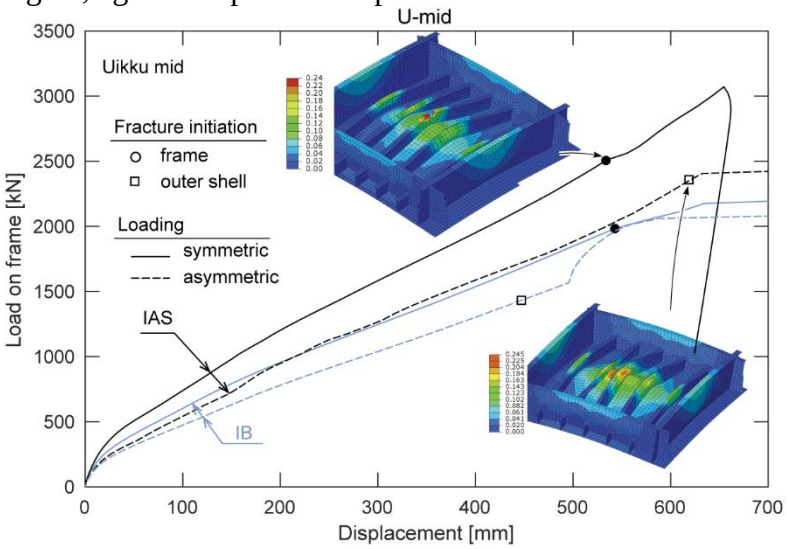

Figure 13. Fracture initiation in structure under pressure load

In above simulations, the middle stiffener remained almost straight exhibiting no tripping nor folding to the sides. This was the main reason which led to high tensile strains in the stiffener flange that ultimately caused the fracture there. Since such a symmetry is almost impossible in reality, another, more probable scenario was analyzed where asymmetry was evoked by off-setting the load 150 mm towards webframe.

Figure 13 clearly shows how irregularity of the load with respect to the frame location is detrimental to the capacity. In both ice classes also fracture load was slightly lower. The most captivating, however, is the fact that for irregular load the fracture took place in the outer shell, rather than in the frames.

6. Frame response

In this section, the behaviour of frames is studied more extensively with the proposed loading scenario as it yields more structural damage and is thus less conservative. Besides Uikku ship, analyses are performed with S.A. Agulhass II. We performed analyses with three ice classes (IA Super, IA and IB) and considered three hull regions: bow, mid and stern.

6.1 Analyzed ship structures

The main particulars of both ships are given in Table 3. The reason why these ships were selected was that the ships were intrumented with strain gages and thus, there exist experimental data we can later compare our analysis results.

S.A. Agulhas II in Figure 14 (a) was built to be classified as Polar ice class PC5 and the hull was constructed in accordance with DNV ICE-10. For the structural scantlings of bow, mid-ship and stern, T-frames are used. The frame span for the bow is 2.065 m and 1.1 m for the mid-ship and stern. The frame spacing and webframe spacing for bow, mid-ship and stern is 0.4 m and 2.4 m respectively. Three areas of the starboard side of the hull were instrumented with strain gauges when it was under construction in 2011/2012. Ice-induced loads were determined by instrumenting the upper and lower parts of the frame with V-shaped strain gauges,

which measured the shear strains occurring in the frame. The instrumentation was applied to two adjacent frames at the bow, three adjacent frames at the bow-shoulder and four adjacent frames at the stern-shoulder. In addition, the hull plating was instrumented with strain gauges in these areas. See Suominen et al. (2013) for more detailed description of the instrumentation.

M/T Uikku in Figure 14 (b), on the other hand, is classified by DNV as class +1 A Tanker for Oil and according to FSICR, it is classified as ice class IA Super. Ship was built in 1976 in Werft Nobiskrug Gmbh, and Helsinki New Shipyard rebuilt Azipod conversion 1993. The ship has a diesel electric propulsion system with four diesel generators. The ship hull and propulsion system was instrumented in 1997 for the EU funded ARCDEV project and the instrumentation was extensive. Measurements were performed on the shell transverse frame at bow area, at bow shoulder area, at midship area and at aftship area (measured by shear strain gauges), load on the shell longitudinal frames at midship area (measured by shear strain gauges), stresses on the shell plating and frames at waterline at bow area, at bow shoulder area, at midship area and at aftship area, the longitudinal bending stresses on deck and vertical accelerations at the bow and stern of the ship and longitudinal acceleration at bow. Thereby, the ice loads were evaluated by measuring shear strains at roughly the neutral axis of the frame. The scantling information for both ships are summarized in the tables below. More detail description of the instrumentation can be found in Kotisalo and Kujala (1999). The frame span for the bow is 2 m, 2.92 m for the bow-shoulder and 1.22 m for the stern, and the frame spacing is 0.35 m.

Table 3. The main particulars of two ships

Ship	Length	Breath	Design draught	Deadweight	Displacement	Service speed	Power
S.A. Agulhass II	121.8	21.7	7.65	5000	13632	14 kn	9 MW
Uikku	150 m	22.2 m	9.5 m	15748 t	22654 t	17 kn	11.4 MW

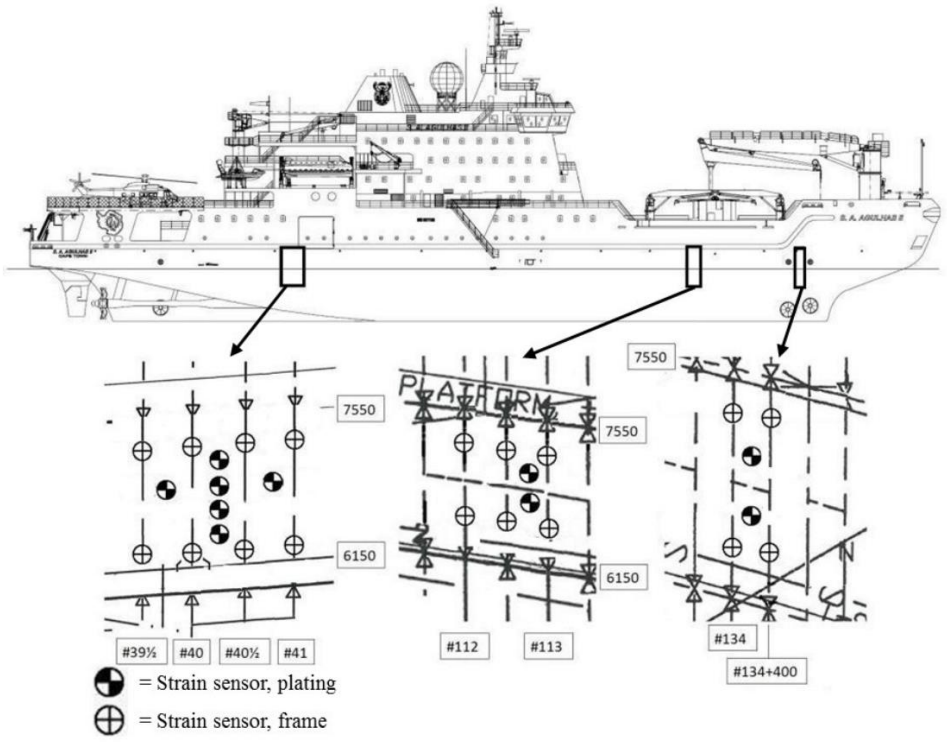

(a)

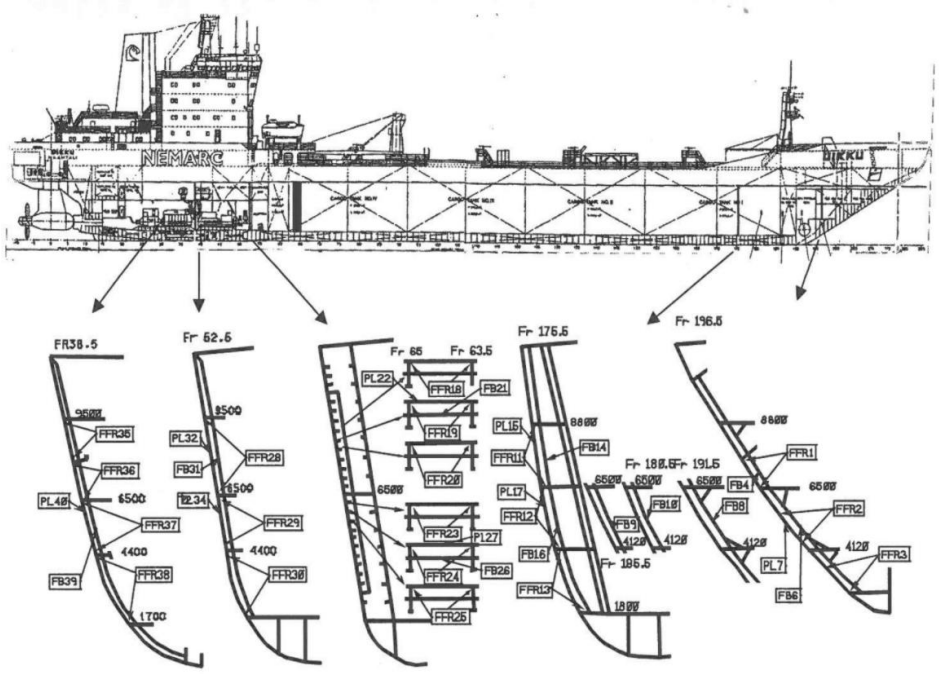

(b)

Figure 14. Pictures of two ships for which measurement data is available.

6.1.1 Approach

The large number of analysis performed required a systematic approach. The process is outlined in Figure 15. The ships have been re-dimensioned to comply with the FSICR requirements. This was done for three ice classes (IA Super, IA and IB) and three hull regions: bow, mid and stern. Scantlings were calculated using FSICR equations and each ship's input dimensions, see Table 4. During scantlings calculations, the brackets have been assumed to be non-existent in the models. Using the obtained scantlings from Matlab, Abaqus python module has been used to build parametric finite element models of both ships. These parametric features provide the swift ability to examine the effects of design changes. Using parametric modeling, a finite element model and its mesh characteristics can be completely defined in terms of parameters or variables. A finite element parametric modeling method of ships overcomes the time-consuming aspect of finite element analysis pre-processing which makes exploring the design space very effective. Furthermore, these scripts are published together with this report which makes them accessible in future investigations.

Thin shell elements have been used to model frames, plating, web frames, flanges and stiffeners. Although stringer and web span are slightly different for both ships, all models include 5 bays in both longitudinal and transverse direction as shown in Figure 4.

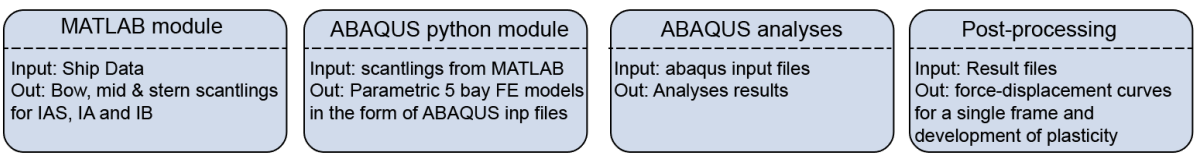

Figure 15. Flow diagram of analysis steps

Table 4. Calculated scantlings for both ships according to FSICR. Yield stress assumed in calculations is 285 MPa.

UIKK	Bow	Plating	Frames [mm] (spacing=0.35m)				stringers [mm] (spacing=2m)				webframes [mm] (spacing=2.8m)				Power
		t [mm]	h_web	t_web	w_flange	t_flange	h_web	t_web	w_flange	t_flange	h_web	t_web	w_flange	t_flange	P [kW]
	IAS	21.5	260	9.5	80	12.5	660	18	140	20	900	15	80	17	11400
	IA	20	260	9	70	11.5	580	16	145	21	700	15	60	15	6614
	IB	19	240	9	70	11.5	540	17	120	18	650	15	80	15	5300
	Mid	Plating	Frames [mm] (spacing=0.35m)				stringers [mm] (spacing=2m)				webframes [mm] (spacing=2.1m)				Power
		t [mm]	h_web	t_web	w_flange	t_flange	h_web	t_web	w_flange	t_flange	h_web	t_web	w_flange	t_flange	P [kW]
	IAS	16	190	9	70	11.5	500	10	60	14	550	13	80	16	11400
	IA	15	170	9	70	11.5	450	8	55	14	450	12	60	15	6614
	IB	12.5	140	9	70	11.5	350	9	60	13	350	12	60	15	5300
	Stern	Plating	Frames [mm] (spacing=0.35m)				stringers [mm] (spacing=1.22m)				webframes [mm] (spacing=2.1m)				Power
		t [mm]	h_web	t_web	w_flange	t_flange	h_web	t_web	w_flange	t_flange	h_web	t_web	w_flange	t_flange	P [kW]
	IAS	14	120	9	40	11.5	450	8	60	14	500	10	80	16	11400
	IA	11.5	100	9	50	10	340	8	80	14	380	10	80	16	6614
	IB	10	80	9	40	10	290	10	40	10	290	10	40	10	5300

Agulh	Bow	Plating	Frames [mm] (spacing=0.43m)				stringers [mm] (spacing=2.065m)				webframes [mm] (spacing=2.4m)				Power
		t [mm]	h_web	t_web	w_flange	t_flange	h_web	t_web	w_flange	t_flange	h_web	t_web	w_flange	t_flange	P [kW]
	IAS	22.5	290	10.5	80	16	600	17	80	21	700	15	80	17	9000
	IA	18.5	210	10	80	15	500	14	75	18	600	12	60	16	4941
	IB	16	170	10	80	15	400	14	70	18	500	12	50	15	3478
	MID	Plating	Frames [mm] (spacing=0.43m)				stringers [mm] (spacing=1.13m)				webframes [mm] (spacing=2.4m)				Power
		t [mm]	h_web	t_web	w_flange	t_flange	h_web	t_web	w_flange	t_flange	h_web	t_web	w_flange	t_flange	P [kW]
	IAS	17	210	10	80	15	500	15	70	17	500	12	70	15	9000
	IA	15	170	10	80	15	400	13	70	16	450	9	60	12	4941
	IB	13	140	10	80	15	350	12	60	14	400	8	55	10	3478
	Stern	Plating	Frames [mm] (spacing=0.43m)				stringers [mm] (spacing=1.13m)				webframes [mm] (spacing=2.4m)				Power
		t [mm]	h_web	t_web	w_flange	t_flange	h_web	t_web	w_flange	t_flange	h_web	t_web	w_flange	t_flange	P [kW]
	IAS	15	170	10	80	15	400	14	70	17	400	12	70	15	9000
	IA	13	140	10	80	15	350	12	70	16	400	9	60	12	4941
	IB	10.5	120	10	80	15	300	9	60	13	300	7	45	9	3478

6.2 Frame analysis results

The results for all analysed cases are shown in Figure 16 presented in the form of load on single frame plotted as a function of displacement. The load on a single frame was preferred over a total load as a comparative measure because this is also available from measurements facilitating the comparison in the sequel. Load on a single frame, that is for one frame spacing, was found by integrating the applied pressure over the corresponding area. Displacements were measured in the plate field at the frame location. The permanent deformations in the structures were determined by assuming that the slope of the unloading curve remains the same due to the permanent nature of plastic strains. Thereby, the unloading portion of the curve is shifted towards left along the x-axes as shown in Figure 6 so that the permanent set would be exactly equal to the reference permanent displacement.

In general, stiffness reduction correlates with the decrease in ice class as well as hull region – this is consistent with the current design approach. On the curves, three distinctive points are marked: load to permanent deformation s/12, design load according to the FSICR and three hinge pressure load (Daley, 2002). Furthermore, from FE simulations we could determine the yield point in each analysis. All the results are combined in Table 5.

The yield capacity is reached before permanent deformation. The last line in Table 5 gives the ratio between the yield load and the design load, i.e. the safety factor against yield – this is presented also in Figure 17 (a). The closer the safety factor is to 1 the more successfully the structure follows the design intention of the FSICR that is reaching the state of yielding when subjected to design pressure. Uikku follows the design intention surprisingly well. The midship and stern regions of Agulhas II are slightly over-dimensioned. The safety factor against permanent deformation of s/12 is larger than ~2.5.

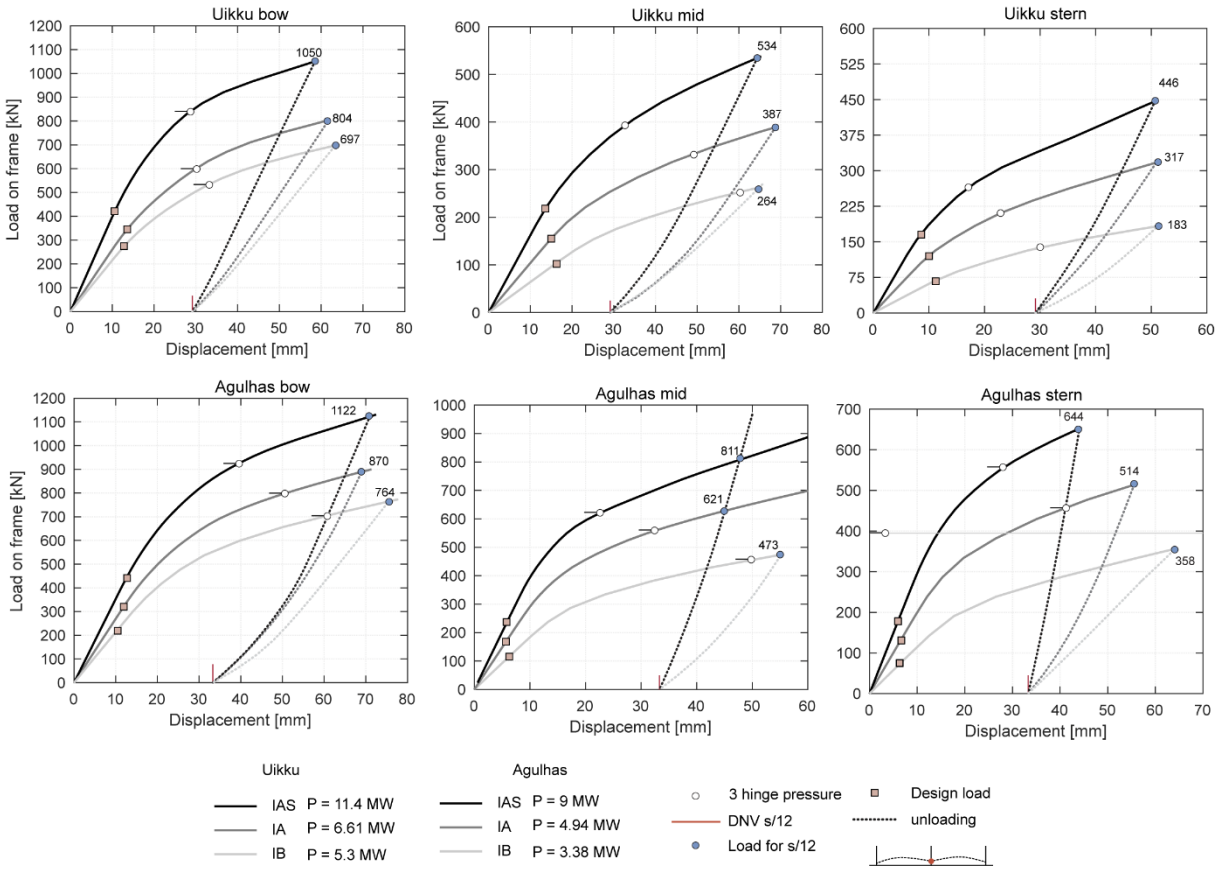

Figure 16. Load-displacement curves for all analysed cases.

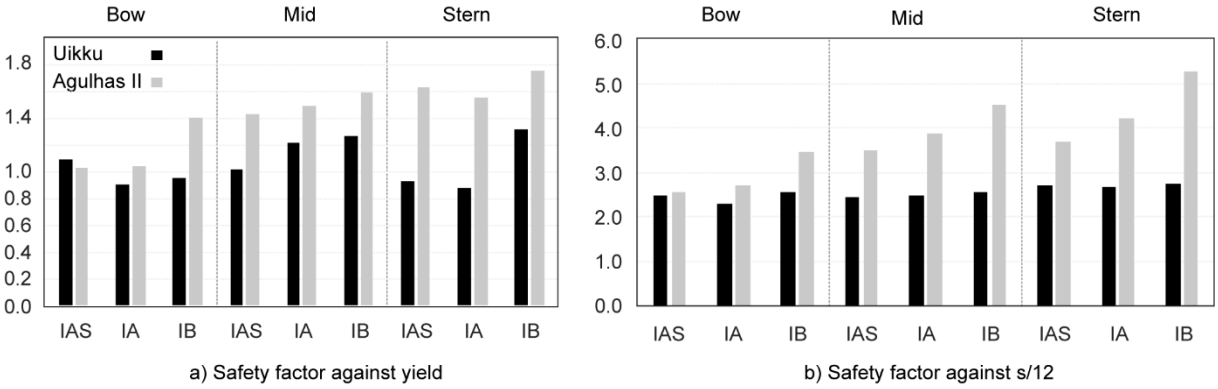

Figure 17. Design safety factor against different capacity levels.

Table 5. Analysis results for Uikku and Agulhas II. Load corresponding to permanent deformation of s/12 and yield compared with design load according to FSICR.

	BOW			MID			STERN		
UIKKU	IAS	IA	IB	IAS	IA	IB	IAS	IA	IB
Load for permanent deformation [kN]	1050	804	697	534	387	264	446	317	183
Yield limit [kN]	461	316	263	221	190	132	154	105	88
Patch area [m2]	0.12	0.11	0.09	0.12	0.11	0.09	0.12	0.11	0.09
Design pressure [MPa]	3.44	3.31	3.13	1.78	1.48	1.18	1.34	1.13	0.76
Design load [kN]	421	348	274	218	155	103	164	119	67
p3h load [kN]	839	602	532	393	333	253	265	210	137
Safety factor against s/12	2.5	2.3	2.5	2.4	2.5	2.6	2.7	2.7	2.8
Safety factor against yield	1.1	0.9	1.0	1.0	1.2	1.3	0.9	0.9	1.3

S.A. AGULHAS II	BOW			MID			STERN		
	IAS	IA	IB	IAS	IA	IB	IAS	IA	IB
Load for permanent deformation [kN]	1122	870	764	812	621	473	644	514	358
Yield limit [kN]	454	334	310	334	239	167	286	191	119
Patch area [m2]	0.14	0.12	0.10	0.14	0.12	0.10	0.14	0.12	0.10
Design pressure [MPa]	3.15	2.68	2.2	1.66	1.33	1.05	1.25	1.02	0.68
Design load [kN]	441	322	220	232	160	105	175	122	68
p3h load [kN]	925	684	502	626	559	461	560	461	395
Safety factor against 3/12	2.5	2.7	3.5	3.5	3.9	4.5	3.7	4.2	5.3
Safety factor against yield	1.0	1.0	1.4	1.4	1.5	1.6	1.6	1.6	1.8

7. Description of full scale measurements

The ice load is determined with the full-scale observations onboard two vessels: Research vessel SA Agulhas II in Antarctica and tanker Uikku in the Russian Arctic. Table 3 and Table 4 summarise the main characteristics of the vessels and Figure 14 illustrates the ships.

7.1 Description of the measuring voyage

7.1.1 SA Agulhas II

Full scale measurement data on ice conditions was collected in the Antarctic waters onboard S.A. Agulhas II between Dec 6, 2013 and Feb 2, 2014. The ice conditions were observed visually and the machinery control and navigational data were recorded continuously. The ice-induced loads were also measured at the bow, bow shoulder and stern shoulder of the ship hull.

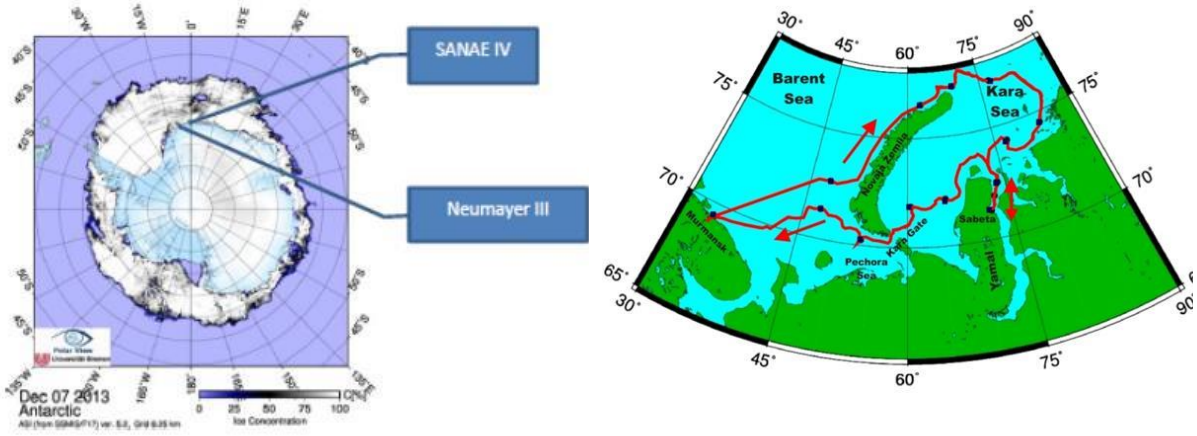

Figure 18. Left: Sea ice extent on Antarctica on 7th December 2013. Right: Route of the convoy during ARCDEV voyage.

The ship departed Cape Town on November 28th, 2013 (Suominen et al., 2015a, 2015b). From Cape Town, the ship headed to the zero Meridian, which she followed to Antarctica, see Figure 18. The first time the ship encountered ice was on December 7th. On December 23rd, the ship arrived the Akta Bukta close to the Neumayer III (the German Antarctic research station, see Figure 18 left).

Between December 24th and 30th, the ship operated between the Akta Bukta and the Penguin Bukta (the location at the ice shelf with the shortest distance to the South African Antarctic research station, SANAE IV, see Figure 18 left) close the ice shelf. On December 30th, the ship headed towards South Georgia and the South Sandwich Islands. The ship arrived at the South Sandwich Islands January 4th when also the extent of sea ice ended.

The ship returned in ice-infested waters January 23rd to get through the pack ice to Penguin Bukta for the passengers and cargo unloading, where she arrived January 25th. The ship operated between the Penguin Bukta and Akta Bukta between January 26th and 31st. The ship headed back to Cape Town on January, 31st and the last ice was observed 1st February.

7.1.2 MT Uikku

The voyage started from the port of Murmansk on 26th of April 1998, so this presents hard winter time ice conditions for the studied area. The route of the convoy is presented in Figure 18 (right) (Kotisalo and Kujala, 1999). Due the heavy ice conditions and the east wind the passage through the Kara Gate was blocked and the convoy – MT Uikku and IB Kapitan Dranitsyn – entered the Kara Sea using the northern route. North edge of the Novaya Zemlja was passed on 29th of April and the nuclear icebreaker Rossiya joined to the convoy.

While the convoy was proceeding through the Kara Sea the IBN Vaygach broke a channel through the fast ice of the bay of Ob to the town of Sabeta. The convoy reached the entrance of this channel on 3rd of May, when the IBN Rossiya left the convoy. MT Uikku and IB Kapitan Dranitsyn proceeded on their own to Sabeta, and the con-voy reached subice loading terminal on 4th of May.

Loading was completed on 8th of May and the convoy proceeded back to the Kara Sea. When the convoy reached the Kara Sea IBN Rossiya joined the convoy and assisted the convoy through the Kara Sea and through the Kara Gate to the Barents Sea, where the convoy arrived on 12th of May. After light ice conditions and open water were reached MT Uikku proceeded independently to Murmansk, where she arrived on 13th of May.

7.2 Observed ice conditions

7.2.1 SA Agulhas II

Ice conditions were observed continuously by visual observations on the ship and reported in 15-minutes intervals during the first day and in 10-minutes intervals thereafter. The ice concentration was observed in tenths during each observation period. The mean ice concentration during each observation period was calculated as a weighted average and the results are presented in Figure 19. The sea ice concentration was high, almost 100 %, most of the time.

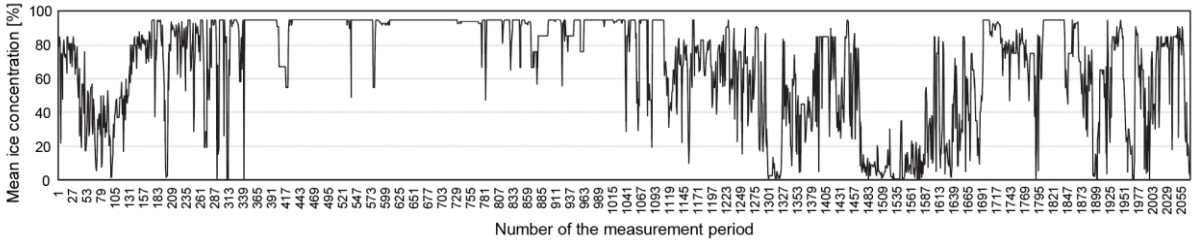

Figure 19. Mean ice concentration in each observation period onboard SA Agulhas II.

Ice thickness was estimated by observing the thickness of the turning ice floes at the bow of the ship both visually and by using stereo-camera photos. Observations of ice thickness have been reported at a 20 cm ice thickness interval from 0 to 2 meters and at 50 cm intervals thereafter for each observation period. This was possible when the ice thickness was up to about 2 m, but when the ice thickness exceeded 2 m, the ice pieces did not turn anymore and the thickness

estimation was more complicated. Thick snow cover made also the thickness observations difficult. Figure 20 shows the observed mean ice thickness for each period.

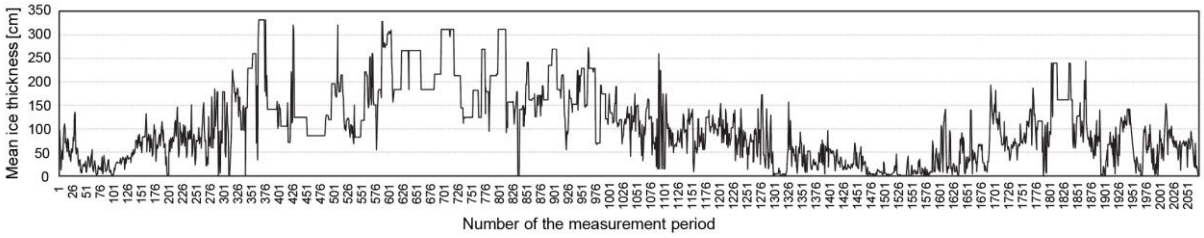

Figure 20. Mean ice thickness in each observation period onboard SA Agulhas II

Most of the time, the level ice thickness encountered at a certain 10-minutes observation period varied quite much. Typically, 4 to 6 different ice thicknesses were observed during each 10-minutes periods. Obviously, the ice fields are often moving out to the open sea from Antarctica due to the wind, waves and currents and therefore the level ice field is broken into ice floes. New ice is then formed between the broken ice floes, which can explain the existence of different thicknesses of level ice at open sea.

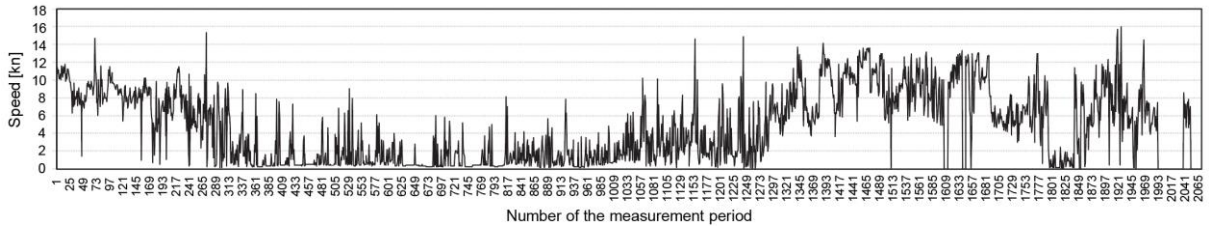

Figure 21. The speed of SA Agulhas II during each 10-minutes period.

Figure 21 illustrates the ship's speed during the voyage. As can be seen, the ship had large difficulties to get through the thick ice regime when approaching Akta Bukta before Christmas 2013. The ship was stuck a number of times, but got however slowly forward independently by ramming through the thick ice.

7.2.2 MT Uikku

Ice conditions were observed continuously by visual observations on the ship and reported in 20 minutes intervals. The ice concentration was observed in tenths during each observation period. The mean ice concentration during each observation period was calculated as a weighted average and the results are presented in Figure 22.

Ice thickness was estimated by observing the thickness of the turning ice floes at the bow of the ship visually. Observations of ice thickness have been reported on five classes: below 10 cm, 10-30 cm, 30-70 cm, 70-120 cm and above 120 cm. Figure 23 shows the observed mean ice thick-ness for each period. Figure 24 illustrates the ship's speed during the voyage. As can be seen, the ship could keep fairly high speed of 10-15 kn most of the time as there were always icebreakers to assist the ship.

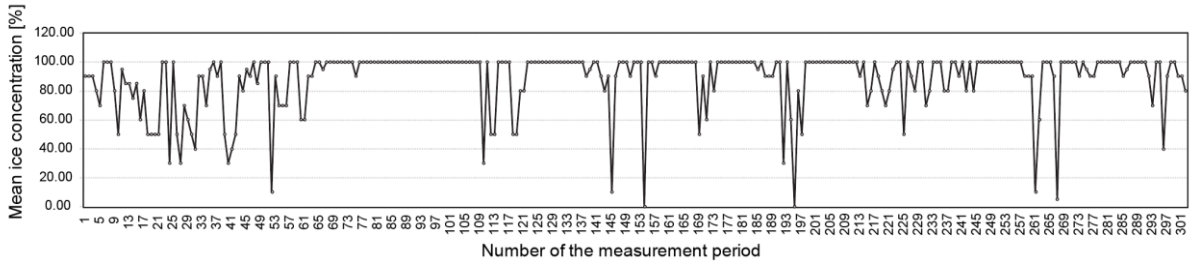

Figure 22. Mean ice concentration in each observation period onboard MT Uikku.

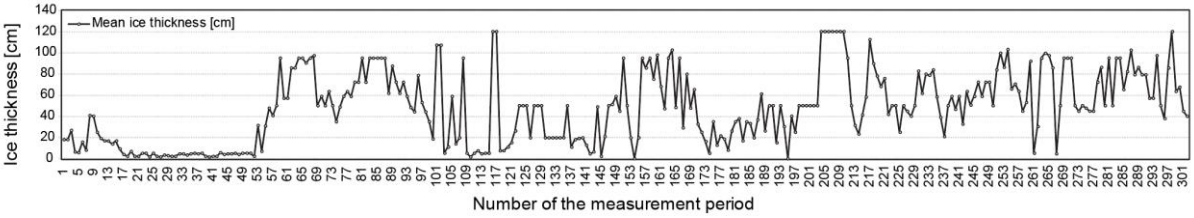

Figure 23. Mean ice thickness in each observation period onboard MT Uikku.

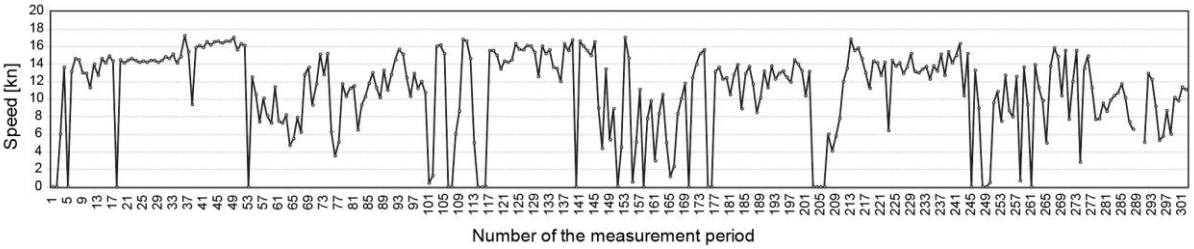

Figure 24. The speed of MT Uikku during each 20-minutes period.

7.3 Evaluation of the design load

7.3.1 SA Agulhas II and MT Uikku

The measured 10-minute maximum loads at the bow and stern are used in this analysis. The data is divided into 4 four classes using ice thickness as the criteria: smaller than 0.7 m, between 0.7-1.2 m, between 1.2-2.0 m and higher than 2.0 m (Kurmiste, 2016). Figure 25-27 summarise the measured load and fitted Gumbel 1 distribution on the data. Gumbel 1 equations can be presented:

$$G(y_n) = \alpha_n e^{-e^{-\alpha_n(y_n - u_n)}} \tag{6}$$

where Gumbel parameter α_n is the inverse measure of dispersion and u_n is the characteristic largest value. These are determined based on the mean μ and standard deviation σ of the measured loads as follows:

$$\alpha_n = \frac{\pi}{\sigma\sqrt{6}} \tag{7}$$

$$u_n = \mu - \frac{\gamma}{\alpha_n} \tag{8}$$

Where γ = 0.577 is the Euler constant. α_n and u_n are parameters used and given also on the Figure 25-27.

Figure 27 shows that the load on the bow shoulder area is almost twice as high as on the bow area. The main reason for this is that the vertical frame angle is much smaller around the frame 176.5 (bow shoulder) than on the frame 196.5 (bow), which will result into higher ice induced loads to break the ice. In FSICR these areas are not separated, therefore in the following analysis, the load measured at the bow shoulder area will be used to evaluate the maximum ice thickness for various ice classes for the bow area. Another reason for the high load at the bow shoulder is that this area encountered more ice hits than the bow itself.

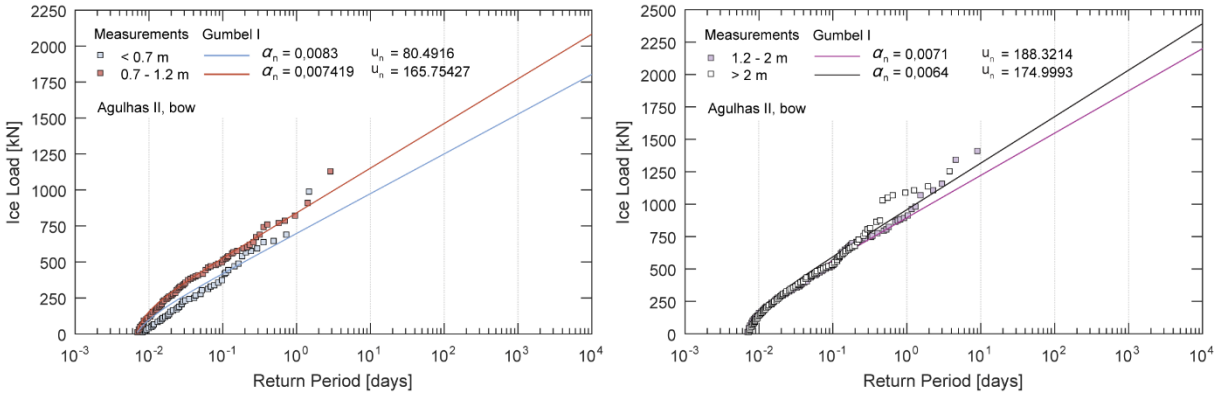

Figure 25. Measure 10 min maxima with fitted Gumbel 1 distribution for SA Agulhass II at bow.

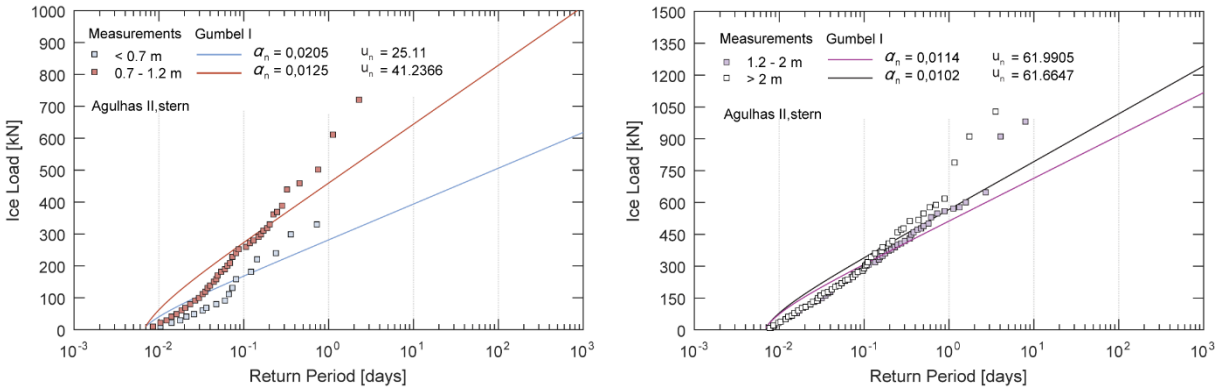

Figure 26. Measure 10 min maxima with fitted Gumbel 1 distribution for SA Agulhass II at stern.

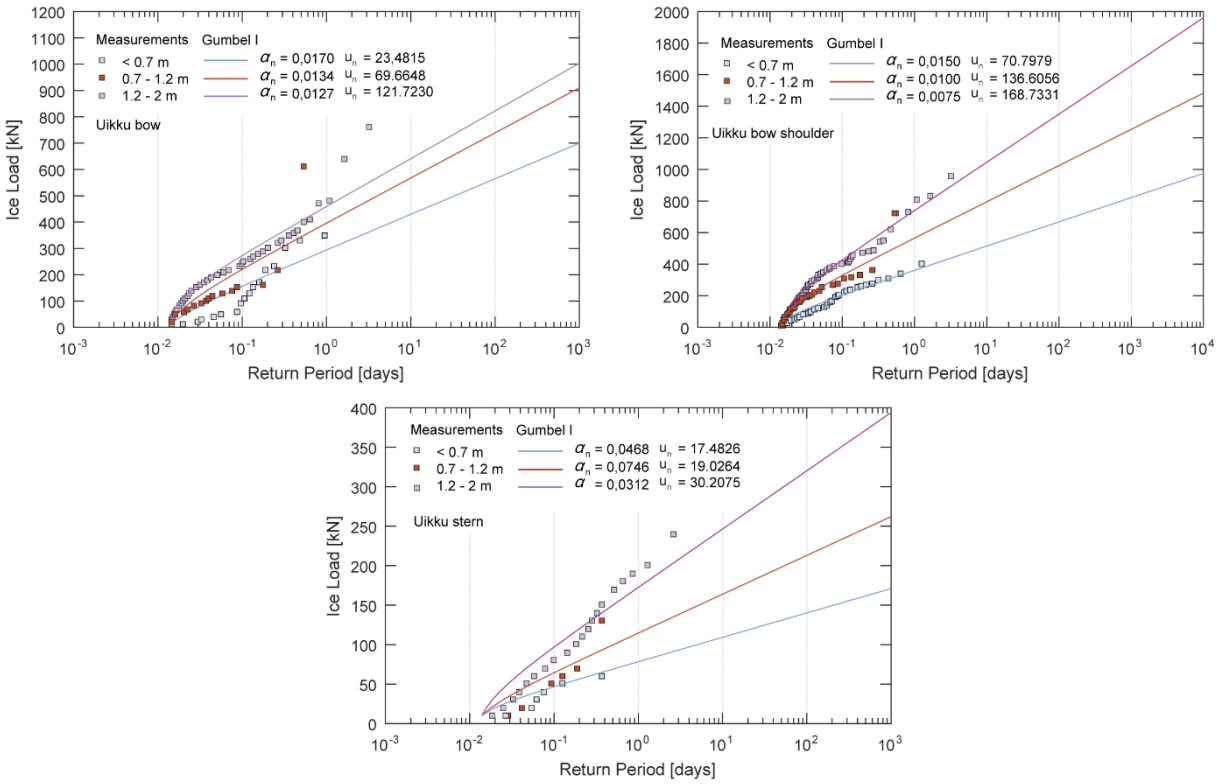

Figure 27. Measure 20 min maxima with fitted Gumbel 1 distribution for MT Uikku fro bow, bow shoulder and stern.

7.4 Evaluation of the design load

The design of structures to withstand the ice loads has to take into account the stochastic nature of this load. Therefore, a rational design procedure necessitates to use a statistical approach of some sort.

Therefore, once the Gumbel parameters *a* and *u* are known, the most probable extreme value with the probability of αs, can be determined:

$$\widehat{y_n} = u - a^{-1} \ln\left(-\ln\left(1 - \frac{\alpha s}{n}\right)\right) \tag{9}$$

Using eq. (8) and the data given in Figures 25-27, the most probable design load values during one voyage (return period one day) are given for two safety levels, namely $\alpha_s = 0.1$ and $\alpha_s = 1$. These safety factors are chosen as they comply with the latest standard for design of Arctic offshore structures (ISO 19906:2010), which defines the three exposure categories and related return period for the probability of occurrence of these:

1. Ultimate limit state (ULS) for all exposure levels (EL's) requires extreme 100-year (10^{-2}) ice event with action factors dependent on the EL. ULS generally correspond to resistance to extreme applied actions.
2. Abnormal/accidental limit state (ALS) for with 1,000 year (10^{-3}) ice events allowing some structural damage but robustness have to be achieved with no loss of life or harm to the environment.
3. Serviceability (SLS) ensuring functionality under any 10 year (10^{-1}) ice event. Exceedance of SLS results in the loss of capability of a structure to perform adequately under normal use.

From the ones presented above we are using SLS criteria ($\alpha_s = 0.1$), which was also used previously to define the load values in Figure 16. Hence, by comparing our analysis results with the most probable loads we can assess under which conditions it is safe to operate, see Figure 28. The curves corresponding to $\alpha_s = 1$ are plotted for reference to show the difference between 10 years and 1 year extreme event (Figure 29).

Figure 28 shows the comparison of ships for safety level of $\alpha_s = 0.1$. For Uikku, long term data is available for three ice thicknesses: <0.7, 0.7-1.2, 1.2-2, thus following values are used in the figure as markers: 0.7, 1.2, and 2 m; respectively, for Agulhas II data is available for four ice thicknesses: <0.7, 0.7-1.2, 1.2-2 and >2 m with respective markers at: 0.35, 0.95, 1.6, 2.5. Dashed lines show the SLS load obtained with FE calculations. Note that Agulhas II experienced slightly higher loads due to the independent operation during measurements, while Uikku operated under icebreaker assistance.

- Performance of ships designed according to IA Super:
  In assisted operation Uikku designed according to IA Super can operate in 2 m thick ice. In contrast, according to Figure 28 (b) Agulhas II (IA Super) can operate independently in 0.35 m thick ice, but if slightly larger permanent deformations are allowed in the bow region, operation in 1 m thick ice is feasible.
- Performance of ships designed according to IA:
  In assisted operation IA design can operate in 1.2 m thick ice. Independent operation is prohibitive as probable loads are higher than load for permanent deformation. However, if slightly higher permanent deformation would be allowed in the bow region (more than s/12), independent navigation upto 0.5 m is possible.
- Performance of ships designed according to IB:
  In assisted operation IB design can operate in 1 m thick ice. Independent operation is prohibitive as experiened loads are higher than load for permanent deformation.

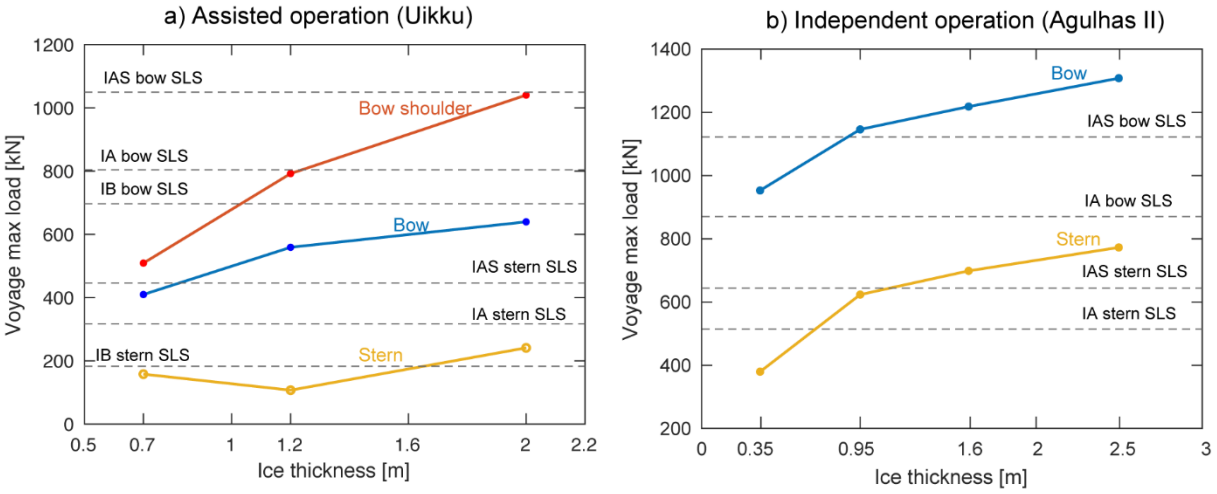

Figure 28. Comparison of measured load with SLS load. Measured data corresponds to safety level of 0.1 (10 years extreme event).

Figure 29 shows the same plots for the safety factor of 1 that corresponds to 1 year extreme event. The most probable loads are lower as expected number of interactions decrease. Recall that according to the FSICR shipstructures are designed to yield once per winter, thus the most probable loads are compared with yield load obtained from FE simulations.

- Performance of ships designed according to IA Super:
  In assisted operation IA Super can operate in 1 m thick ice, but independent operation is prohibitive.

- Performance of ships designed according to IA:
  In assisted operation IA can operate in 0.7 m thick ice with some yielding taking place in bow shoulder. Independent operation is prohibitive.
- Performance of ships designed according to IB:
  In assisted operation IB can also operate in 0.5 m thick ice, with some yielding taking place in bow shoulder and stern region. Independent operation is prohibitive.

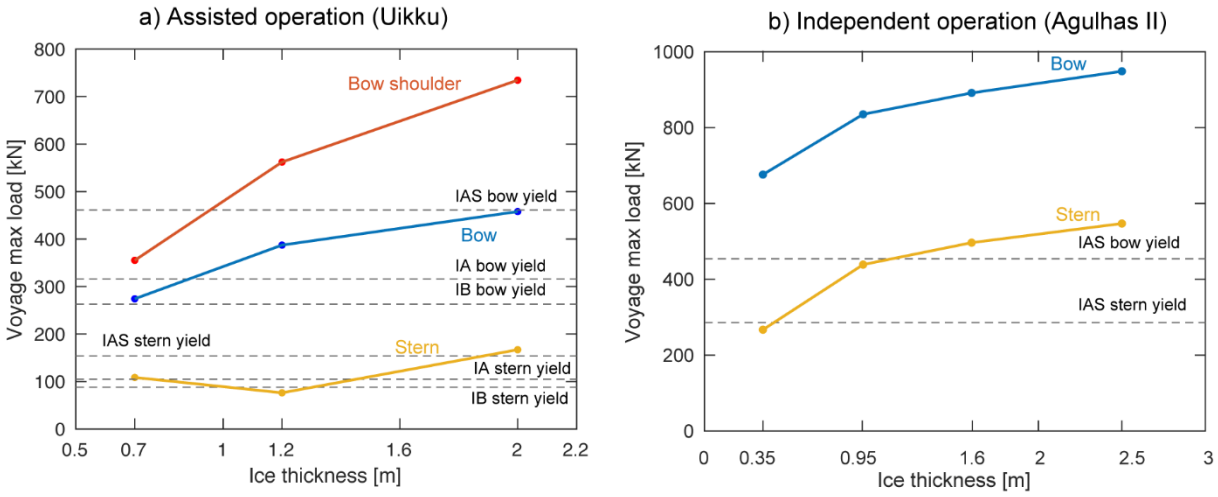

Figure 29. Comparison of measured load with yield load. Measured data corresponds to safety level of 1 (1 years extreme event).

8. Comparison of results with preliminary assessment in Polar Code

IMO has adopted the International Code for Ships Operating in Polar Waters (Polar Code) and related amendments both to the International Convention for the Safety of Life at Sea (SOLAS) and the International Convention for the Prevention of Pollution from Ships (MARPOL) to make the Polar Code mandatory. One of the aspects of the Polar Code addresses the operational limitations of ships of different categories (A, B and C) according to ice conditions. The approach for evaluating the ice conditions and setting limitations for ships assigned an ice class is called POLARIS – Polar Operational Limit Assessment Risk Indexing System, details of which are given in MSC.1/Circ.1519 (2016). Therein the ice classes are associated with the limiting ice thickness by combining the experience from three existing approaches used in ice-covered waters: the Canadian Arctic, the Baltic (Finnish/Swedish), and the Russian Northern Sea Route systems. The assessment given in MSC 94 (2014) categorizes ships designed according to the Finnish Swedish Ice Class Rules (FSICR) for different operational conditions. Here, the validity of this preliminary assessment is discussed in the light of the results presented in the previous Section.

8.1 Limitations

Before discussing the validity of the preliminary assessment, it is important to highlight the limitations of the present findings. First, the measurement data is never as exhaustive as it could be – this applies to the data used herein as well. Agulhas II data is based on one voyage making the long-term predictions less reliable. During the measurement period Uikku operated 2 weeks in rather extreme conditions that could lead to higher load levels than usually experienced. Moreover, the amount of data is scarce for Uikku as the voyage was only 2 weeks long. In addition, the loading data was gathered only in 20 minute intervals – decreasing the interval would have doubled the amount of data.

Furthermore, both ships have an icebreaking hull form that means that the ice breaking process is more efficient and experienced loads potentially lower compared to hull forms, which are optimized for sailing in open water, e.g. hull forms with a bulbous bow. The design requirements of the FSICR, however, do not take the hull form into account and thus, in the analyses, structures were assumed vertical.

Related to numerical simulations there are two major uncertainties: 1) the neglection of brackets in FE models and 2) the assumed non-uniform pressure profile applied to the structure. The former presumably makes the structures slightly weaker, so there is additional implicit safety margin built into the analysis results. The latter, as demonstrated in Section 4, reduces stiffness compared with the design approach of the FSICR. In effect, the combination of these two assumptions can potentially cancel each other as modelled brackets would have reduced deformations, while non-uniform pressure patch increased deformations.

8.2 Assisted operation

In POLARIS system, the operational restrictions are based on the definitions given in the Ice Nomenclature of WMO. Safe operational ice conditions for assisted operation in first-year ice are given in Table 6 together with the assessment made in this study (safety level of 0.1). Comparison reveals that the preliminary assessment is more conservative, especially for higher ice

classes. For IB ice class, the current extensive simulation based assessment gives only a 10 cm thinnerlimiting ice thickness value than the preliminary assessment.

Table 6. Comparison between the preliminary assessment from POLARIS and the assessment done in this study for safe operation of ships in first-year winter ice regime for the Finnish-Swedish ice classes, when icebreaker assistance is provided or the ice concentration is less than 100%. SLS means the serviceability limit state.

POLARIS assessment (Polar Code)			Current assessment [cm]	
Ice class	WMO description of the ice regime	Thickness of ice floes, hi	SLS	Yield
IA Super	Medium first-year ice	hi up to about 100 cm	200 cm	100 cm
IA	Medium first-year ice	hi up to about 80 cm	120 cm	70 cm (some yielding)
IB	Thin first-year ice	hi up to about 60 cm	100 cm	50 cm (some yielding)
IC	Thin first-year ice	hi up to about 40 cm	-	-

8.3 Independent operation

According to the POLARIS system the Polar Ship Certificate given for independently operating ships in first-year ice imposes operational limitations only based on ice thickness, and not by ice concentration, see Appendix A.

Current results are consistent with the preliminary assessment made in POLARIS for ice classes IA Super and IA, but operation by IB class vessel is prohibitive, see Table 7.

Table 7. Comparison between th preliminary assessment from POLARIS and the assessment done in this study for safe operation of ships in first-year winter ice regime for the Finnish-Swedish ice classes during independent operation.

Polaris assessment			Current assessment [cm]
Ice class	WMO description of the ice regime	Thickness of ice floes, hi Ice concentration, Ci up to 100%	
IA Super	Medium first-year ice	hi up to about 80 cm	100 cm
IA	Medium first-year ice	hi up to about 70 cm	50 cm
IB	Thin first-year ice	hi up to about 50 cm	prohibitive
IC	Thin first-year ice	hi up to about 30 cm	-

9. Conclusions

This study had two important objectives: first, analyse the limit states of frame and plating and second, assess the validity of the preliminary assessment of the operational restrictions for ships ice-strengthened in accordance with different Finnish-Swedish Ice Classes.

The limit state analysis showed that boundary conditions as well as load application has an important consequence on the load levels. Load applied according to the FSICR via uniform pressure patch resulted in the lowest frame stiffness, but the corresponding line load was significantly higher, and less consistent with measured line load values than some of the alternative load patches used. Therefore, to manifest large deformations on structures, but keep the compliance with measured line load values, a non-uniform pressure patch was used to determine the permanent deformations in the structure.

The load height, i.e. line-like contact as opposed to current design approach, was shown to significantly reduce the capacity of a single frame while the effect on total structural stiffness was insignificant. This leads to two conclusions. First, as the effect was so strong, the results would have been much more conservative than presented in the previous section. Therefore, to keep compliance with present design approach, we did not use this approach in evaluating the

response of frames. Second, it also leads us to think how the total load should be interpreted in terms of frame response. Here, the load on single frame was obtained by integrating the applied load over the frame spacing. In contrast, experimental values are obtained via the shear gauges attached on the both ends of the frame, and by the measured shear strain difference. Future investigations should consider this aspect when presenting "load on frame".

Consequently, the proposed NUPP loading scenario was used with a load height consistent with the present design rules to determine the serviceability limit state (SLS) of two ships designed according to three ice classes: IA Super, IA and IB. The permanent set limit of s/12 given by DNV was used as a SLS and the load causing this was defined using non-linear FE simulations.

The two ships were chosen as the long-term measurement data was available for these ships and the ships represented two alternative operating regimes: independent operation (SA Agulhas II) and operation assisted with icebreakers (Uikku). Therefore, we could compare the most probable loads experienced by ships estimated by using long-term measured data with our analysis results. The probability of the load was associated with safety factor of 0.1 and 1. The safety factor of 0.1 is consistent with SLS design standard to ensure functionality under any 10-year ice event and safety factor of 1 ensures functionality under one year extreme event, which according to the FSICR is the state of yielding.

This comparison reveals the maximum ice thickness for assisted and independent operation for different ice classes, or in other words, defines the operational limitiations for ice strengthened ships designed according to the FSICR. Similar preliminary assessment of limiting ice thicknesses for safe operation are given in the Polar Code, but without supporting FE analysis. When serviceability is considered as a limiting condition for safe operation, results encouragingly show that the present designs are safer than assumed in the Polar Code when operating under icebreaker assistance or when ice concentration is less than 100%. This extra safety depends on the ice class, with IA Super showing the largest safety margin. When conservatively associating yield with the safe operation, the limiting ice thicknesses provided by POLARIS correlates well with the present findings. Still, it is important to highlight the fact that Uikku has multifunctional icebreaking hull form which possibly decreases the measured loads. Nevertheless, results can be generalized to blunt hull forms as the largest measured loads are measured on the shoulder area, where the frame angle is not substantially different between a multifunctional icebreaking hull and a blunt hull. Independent operation however, is according to our assessment quite consistent with Polar Code assessment when the permanent deflection limit state of s/12 is used.

References

Abraham, J., 2008. PLASTIC RESPONSE OF SHIP STRUCTURE SUBJECTED TO ICE LOADING. Master thesis, Memorial University of Newfoundland.

Abraham, J., Daley, C.G., 2009. Load Sharing in a Grillage Subject to Ice Loading, Presented at the RINA International Conference on Ship and Offshore Technology, Ice Class Vessels. Busan, Korea., pp. 1–5.

ABS 2014. Guidance notes on ice class. American Bureau of Shipping.

Daley, C.G., 2002. Derivation of plastic framing requirements for polar ships. Mar. Struct. 15, 543–559.

Daley, C.G., 2007. Reanalysis of ice pressure-area relationships. Marine Technology 44, 234–244.

Erceg, B., Taylor, R. & Ehlers, S., 2014. A Response Comparison of a Stiffened Panel Subjected to Rule-Based and Measured Ice Loads. In: Proceedings of the ASME 2014 33rd International Conference on Ocean, Offshore and Arctic Engineering, OMAE2014 June 8-13, 2014, San Francisco, California, USA.

Hogström, P., Ringsberg, J.W., Johnson, E., 2009. An experimental and numerical study of the effects of length scale and strain state on the necking and fracture behaviours in sheet metals. Int. J. Impact Eng. 36, 1194–1203. doi:10.1016/j.ijimpeng.2009.05.005

IACS, 2011. Unified Requirements for Polar Ships: I2 - structural requirements for Polar Class ships. International Association of Classification Societies.

ISO 19906:2010, Petroleum and natural gas industries - Arctic offshore structures. Section 7: Reliability and limit state design.

ISSC 2015, 19th INTERNATIONAL SHIP AND OFFSHORE STRUCTURES CONGRESS, Committee V.6 Arctic Technology, Edited by Soares, C.G. & Garbatov,Y. CRC Press.

Jordaan, I.J., Singh, S.K., 1994. Compressive ice failure: critical zones of high pressure. IAHR Ice Symposium, Trondheim, Norway, pp. 505–514.

Kotisalo, K., and Kujala, P. 1999. Ice load measurements onboard MT Uikku during the ARCDEV voyage, 2013. POAC'99, proceedings, Vol 3, Espoo, pp. 974-987.

Kujala, P. and Vuorio, J. 1986. Results and statistical analysis of ice load measurements on board icebreaker Sisu in winters 1979 to 1985," Finnish Board of Navigation, Winter navigation Research Board, Research report No 43, 1986.

Kurmiste, A. (2016). "Analysis of structural safety of ice-going vessels in the Arctic and Antarctic". Master thesis. Aalto University, School of Engineering.

Lepik, K., Peetsalu, J., Viljakainen, S., and Voog, V. 2010. Allowable plate deflections according to DNV.

Lyngra, N.H.L., 2014. Analysis of Ice-Induced Damages to a Cargo Carrier and Implications wrt. Rule Requirements. Master thesis. Norwegian university of Science and Technology, NTNU.

MSC.1/Circ.1519 (2016). Guidance on Methodologies for assessing Operational Capabilities and Limitations in Ice. International Maritime Organization, 2016.

MSC 94/INF.13 (2014). Technical background to POLARIS. Submitted by Canada, Finland, Sweden and the International Association of Classification Societies (IACS). 94th session of the Maritime Safety Committee of IMO, 2014.

Quinton, B.W.T., Daley, C.G., Gagnon, R.E., 2010. Effect of Moving Ice Loads on the Plastic Capacity of a Ship's Structure. In: International Conference and Exhibition on Performance of Ships and Structures in Ice (ICETECH 2010), September 20-23, Anchorage, Alaska.

Quinton, B.W.T., Daley, C.G., Gagnon, R.E., 2012. Realistic Moving Ice Loads And Ship Structural Response, in: Proceedings of the Twenty-second (2012) International Offshore and Polar Engineering Conference Rhodes, Greece, June 17-22.

Riska, K. and Kämäräinen, J. 2012. Comparison of Finnish-Swedish and IACS Ice Class Rules. The Royal Institution of Naval Architects. The Ice Class Ships, 4-5 July 2012, London, UK.

Riska, K., Kämäräinen, J., 2011. A review of ice loading and the evolution of the finnish-swedish ice class rules. Proceedings of the SNAME Annual Meeting.

Suominen, M, and Kujala, P. The Measured Line Load As A Function Of The Load Length In The Antarctic Waters. Proceedings of the 23rd International Conference on Port and Ocean Engineering under Arctic Conditions. 2015.

Suominen, M., et al. 2013. FULL-SCALE MEASUREMENTS ON BOARD PSRV S.A. AGULHAS II IN THE BALTIC SEA 1–12. POAC'13, proceedings.

Suominen, M., Kujala, P. 2015. THE MEASURED LINE LOAD AS A FUNCTION OF THE LOAD LENGTH IN THE ANTARCTIC WATERS, in:. Presented at the Proceedings of the 23rd International Conference on Port and Ocean Engineering under Arctic Conditions, POAC'15.

Suominen, M., Kujala, P., Kotilainen, M., 2015. THE ENCOUNTERED EXTREME EVENTS AND PREDICTED MAXIMUM ICE-INDUCED LOADS ON THE SHIP HULL IN THE SOUTHERN

OCEAN , in:. Presented at the Proceedings of the ASME th International Conference on Ocean, Offshore and Arctic Engineering OMAE May 31-June 5, St. Johns, Newfoundland, Canada.

Appendix A. Excerpt from MSC 94/INF.13 (2014).

8 Safe operational ice conditions for ships ice-strengthened in accordance with FSICR

It may be reasonable to base the operational restrictions on the definitions given in the Ice Nomenclature of WMO. The operational restrictions should be user-friendly, so that the Master of the ship is able to determine the existing ice conditions e.g. from available ice charts. Information provided in this chapter is valid for ships ice-strengthened in accordance with FSICR, 1971, having transverse frames and for all ships ice strengthened in accordance with FSICR, 1985, or later.

8.1 Safe operational ice conditions in first-year ice

Safe operational ice conditions could be given separately for independent operation in first-year ice, and for operation assisted by an icebreaker.

8.1.1 Safe operational ice conditions for independent operation in first-year ice

It is suggested that in ice conditions consisting solely of first-year ice, only the thickness limit of the level ice floes should be given in the Polar Ship Certificate, see Tables 10 and 11. Before contact with ice of half of the ice thickness given in Table 10, the speed of the ship should be limited to 13 kn.

Table 10. Safe operation of ships for independent operation in first-year winter ice regime at open sea for the Finnish-Swedish ice classes. Thickness of level ice floes for independent operation in first-year ice may be lower than given below due to the ship's limited ice-going capability.

Ice class	WMO description of the ice regime	Thickness of ice floes, h_i Ice concentration, C_i
IA Super	Medium first-year ice	h_i up to about 80 cm, C_i up to 100%
IA	Thin first-year ice	h_i up to about 70 cm, C_i up to 100%
IB	Thin first-year ice	h_i up to about 50 cm, C_i up to 100%
IC	Grey-white ice	h_i up to about 30 cm, C_i up to 100%

8.1.2 Safe operational ice conditions for operation when assisted by an icebreaker in first-year ice

Table 11. Safe operation of ships in first-year winter ice regime for the Finnish-Swedish ice classes, when icebreaker assistance is provided or the ice concentration is less than 100%.

Ice class	WMO description of the ice regime	Thickness of ice floes, h_i
IA Super	Medium first-year ice	h_i up to about 100 cm
IA	Medium first-year ice	h_i up to about 80 cm
IB	Thin first-year ice	h_i up to about 60 cm
IC	Thin first-year ice	h_i up to about 40 cm